

An Allen–Cahn approach to the remodelling of fibre-reinforced anisotropic materials

Original

An Allen–Cahn approach to the remodelling of fibre-reinforced anisotropic materials / Grillo, Alfio; Carfanga, Melania; Federico, Salvatore. - In: JOURNAL OF ENGINEERING MATHEMATICS. - ISSN 0022-0833. - STAMPA. - 109:1(2018), pp. 139-172. [10.1007/s10665-017-9940-8]

Availability:

This version is available at: 11583/2683512 since: 2020-06-02T19:45:07Z

Publisher:

Springer

Published

DOI:10.1007/s10665-017-9940-8

Terms of use:

This article is made available under terms and conditions as specified in the corresponding bibliographic description in the repository

Publisher copyright

Springer postprint/Author's Accepted Manuscript

This version of the article has been accepted for publication, after peer review (when applicable) and is subject to Springer Nature's AM terms of use, but is not the Version of Record and does not reflect post-acceptance improvements, or any corrections. The Version of Record is available online at: <http://dx.doi.org/10.1007/s10665-017-9940-8>

(Article begins on next page)

An Allen-Cahn Approach to the Remodelling of Fibre-Reinforced Anisotropic Materials

Alfio Grillo · Melania Carfagna ·
Salvatore Federico

Received: date / Accepted: date

Abstract We propose a theory of remodelling in fibre-reinforced biological tissues, in which the fibre orientation follows a given probability density. The latter is characterised by variance and mean angle. We claim that the fibres may change their orientation in time, thereby triggering a remodelling process that can be described by the spatiotemporal evolution of the mean angle. This is determined by solving a balance of external and internal generalised forces. We assign the latter ones by establishing a constitutive theory capable of resolving the spatial variability of the fibre mean angle, and featuring a free energy density of the Allen-Cahn type. Through numerical simulations, we compare the predictions of our model with the results of another model available in the literature. Finally, we interpret the evolution of the mean angle as the consequence of a symmetry breaking that occurs in the tissue both spontaneously and due to the coupling between remodelling and deformation.

Keywords Porous Media · Biological tissue · Biphasic material · Fibre-reinforcement · Transverse isotropy · Remodelling · Structural changes

This work has been supported in part by the *Politecnico di Torino* (Italy) [AG and MC], in part by the *Fondazione Cassa di Risparmio di Torino* (Italy), through the *La Ricerca dei Talenti* (“HR Excellence in Research”) programme [AG and MC] and in part by the Natural Sciences and Engineering Research Council of Canada, through the NSERC Discovery Programme [SF].

A. Grillo (Corresponding Author) · M. Carfagna
Dept of Mathematical Sciences (DISMA) “G.L. Lagrange”, Politecnico di Torino
Corso Duca degli Abruzzi 24, 10129, Torino, Italy
Tel.: +39-011-0907531. Fax: +39-011-0907599
E-mail: alfio.grillo@polito.it
E-mail: melania.carfagna@polito.it

S. Federico
Dept of Mechanical and Manufacturing Engineering, The University of Calgary
2500 University Drive NW, Calgary, AB, T2N 1N4, Canada
E-mail: salvatore.federico@ucalgary.ca

1 Introduction

Following Cowin’s terminology [1], a biological tissue is “*a collection of cells*” embedded in an extracellular matrix (ECM). Among the constituents of the ECM, elastin and collagen fibres play an essential role in determining the mechanical properties of tissues.

In order to understand how a tissue is generated, how it works, and how it adapts itself to external stimuli, it is necessary to know the internal structure of the tissue itself and the mechanical behaviour of its constituents. Of particular relevance is the study of the ECM, whose properties are tightly related to the presence of elastin and collagen fibres, and to their spatial orientation. In the case of blood vessels, several mathematical models of the tissue’s mechanics have been elaborated, in which a discrete number of families of fibres is considered (see, e.g., [2–6]). Moreover, models that consider statistically oriented fibres have been proposed for various tissues, for example, in [7–10]. To account for the fibres in the constitutive description of biological tissues, the structure tensor is included in the determination of stress through the introduction of suitable invariants of the Cauchy deformation tensor [2, 11, 12].

When the ECM is permeated by an interstitial fluid, the pattern of fibre orientation influences the motion of the fluid by either facilitating or hindering its flow. For instance, this is the case of articular cartilage, whose permeability in the superficial zone should be higher than it actually is, based solely on considerations on the proteoglycan volumetric fraction, as observed by Maroudas and Bullough [13]. Maroudas and Bullough [13] also inferred that this behaviour was likely due to the collagen fibres, which, in the superficial zone, are oriented parallel to the surface and therefore constitute a further obstacle to fluid flow. A possible explanation of this occurrence has been presented in [9]. Subsequently, by putting together the non-linear elasticity model presented in [14], and extending to large deformations the permeability model developed in [15], a general, finite-deformation model was introduced in [16]. In this series of papers, the fibres are assumed to be oriented statistically according to a probability density capable of mimicking the histological pattern observed by other authors [17, 18].

When a tissue deforms, its mechanical properties evolve in time. The deformation, indeed, drives the reorientation of the fibres, thereby modulating the mechanical behaviour of the tissue also in response to the changes in its internal structure. If the deformation is the only responsible for this structural reorganisation, the evolution of the fibre pattern may be said to be a *passive consequence* of the deformation. If, however, as suggested in [19], a tissue is supposed to possess also structural degrees of freedom, which exist independently of deformation, then the reorientation of the fibres becomes part of the tissue dynamics, and it *interacts* with the deformation and stress. This interaction, in turn, may manifest itself in several ways, among which a relevant one is given by the identification of a *stress-driven* pattern of fibre arrangement.

Motivated by the aforementioned considerations, the scope of this work is to propose a model of structural adaptation in fibre-reinforced biological

tissues. In the present framework, the “structural adaptation” is assumed to consist of a variation of the material properties that determine the local orientation of the fibres in a fibre-reinforced soft tissue [20,21]. More specifically, we consider a simplified theoretical setting, in which the only interactions experienced by the tissue arise due to mechanical stimuli, and the tissue itself is hyperelastic. Moreover, no inelastic distortions are considered. Hence, the reorientation of fibres is assumed not to be accompanied by growth, resorption, or any other process of this kind. Still, dissipative entities yielding the variation of the tissue’s internal structure are taken into account. Following the line of thought put forward in [22,23], a probability distribution of the fibre orientation is prescribed, whose functional law features a family of parameters depending on the material points and on time. These parameters shall be referred to as *remodelling variables* in the sequel. While the dependence of the remodelling variables on the material points is related to the inhomogeneity of the tissue, their dependence on time is introduced here in order to allow for their evolution, which is understood as a manifestation of the tissue’s structural adaptation. On this footing, we present a theory of remodelling that, starting from the setup outlined in [22,23], relies on the introduction of a free energy density of the Ginzburg-Landau [24,25] or Allen-Cahn [26] type, and accounts explicitly for the spatial resolution of the remodelling variable¹.

As done in [27,22,23], the hypothesis is made that the remodelling variables are indeed “kinematic variables”, for which suitable balance laws should be introduced in conjunction with the balance laws typically adopted in the continuum mechanics of simple bodies. In this respect, this vision of structural adaptation takes large inspiration from the models of Cermelli et al. [28] and DiCarlo and Quilgotti [19], in which the concept of a “two-layer dynamics” is thoroughly explained.

Previous studies on remodelling have been conducted by many other authors. For example, the interplay between the fibre alignment in fibre-reinforced media and other aspects of the tissue mechanics has been highlighted in [29], while remodelling in collagen gels and tissues with collagenous reinforcement has been studied in [30]. In a slightly different context, a possible coupling between fibre reorientation and growth has been proposed in [31], in conjunction with the Bilby-Kröner-Lee decomposition. Furthermore, the remodelling of the collagen fibres has been addressed also in [32], and the compaction of collagen gels has been studied in [33]. Recently, the influence of the collagen fibres on the mechanics of the aorta has been studied in [34–36].

The remainder of this work is organised as follows. In Section 2, we introduce the dynamics of remodelling. In Section 3, we establish the constitutive framework. In Section 4, we study in detail the remodelling equation, and discuss its asymptotic behaviour. In Section 5, we comment the results of the numerical simulations. Finally, in Section 6, we summarise the key-points of our work, and propose an outline for future research.

¹ The idea was suggested by Prof. Gaetano Giaquinta to S. Federico, S.-K. Han, and A. Grillo during the visit of S.-K. Han to the University of Catania, in 2004, while discussing about the histology of articular cartilage.

2 General mathematical model

We consider a fibre-reinforced porous medium, in which the reinforcing fibres are oriented statistically according to some suitable probability density. To formalise the mathematical description of media of this type, we refer to the works [37, 16, 38–40], which we briefly summarise here. Within the present theoretical framework, the tissue is regarded as a biphasic medium comprising a fluid and a solid phase. The solid phase is the representation of a porous medium, which is assumed to consist of a matrix of biological polymers (e.g., proteoglycans in the case of articular cartilage) and a network of collagen fibres.

2.1 Theoretical background

At the scale at which our theory is formulated, the matrix and the collagen fibres constitute a mixture, in which they are present with volumetric fractions ϕ_{0s} and ϕ_{1s} , respectively. The sum $\phi_s = \phi_{0s} + \phi_{1s}$ defines the volumetric fraction of the solid phase as a whole and, since the saturation condition is assumed to apply, the volumetric fraction of the fluid phase coincides with the porosity of the medium and is given by $\phi_f = 1 - \phi_s$.

The portion of the three-dimensional Euclidean space, \mathcal{S} , occupied by the tissue at time t is said to be the *current configuration* of the tissue. We also introduce a reference configuration, \mathcal{B} . For $x \in \mathcal{S}$ and $X \in \mathcal{B}$, we consider the tangent spaces $T_x\mathcal{S}$ and $T_X\mathcal{B}$, and the co-tangent spaces $T_x^*\mathcal{S}$ and $T_X^*\mathcal{B}$. Moreover, we denote by $T\mathcal{S} = \sqcup_{x \in \mathcal{S}} T_x\mathcal{S}$ and $T\mathcal{B} = \sqcup_{X \in \mathcal{B}} T_X\mathcal{B}$ the tangent bundles of \mathcal{S} and \mathcal{B} , and by $T^*\mathcal{S} = \sqcup_{x \in \mathcal{S}} T_x^*\mathcal{S}$ and $T^*\mathcal{B} = \sqcup_{X \in \mathcal{B}} T_X^*\mathcal{B}$ their co-tangent bundles, respectively [41]. Finally, the space \mathcal{S} and the reference configuration \mathcal{B} are endowed with the metric tensors \mathbf{g} and \mathbf{G} , respectively.

In the present framework, matrix and fibres are assumed to share the same motion. This hypothesis allows to describe the motion of the solid phase by means of a one-parameter family of smooth embeddings. At each time t , the embedding $\chi(\cdot, t)$ maps the points of \mathcal{B} into \mathcal{S} (see [37, 38] for details), i.e.,

$$\chi(\cdot, t) : \mathcal{B} \rightarrow \mathcal{S}, \quad X \in \mathcal{B} \mapsto x = \chi(X, t) \in \mathcal{S}. \quad (1)$$

The tangent map $T\chi(X, t) = \mathbf{F}(X, t) : T_X\mathcal{B} \rightarrow T_{\chi(X, t)}\mathcal{S}$ is the deformation gradient tensor of the solid phase [41], while $\mathbf{C} = \mathbf{F}^T \mathbf{g} \mathbf{F}$ and $\mathbf{b} = \mathbf{F} \mathbf{G}^{-1} \mathbf{F}^T$ denote the right and the left Cauchy-Green deformation tensor, respectively. In order for $\chi(X, t)$ to be admissible, $\mathbf{F}(X, t)$ is required to have strictly positive determinant, $J(X, t) = \det \mathbf{F}(X, t)$, at all points and at all times.

To complete the kinematic description of the considered porous medium, we introduce the velocities of the solid and fluid phase, \mathbf{v}_s and \mathbf{v}_f , the *filtration velocity* $\mathbf{q} = \phi_f \mathbf{w}$, with $\mathbf{w} = \mathbf{v}_f - \mathbf{v}_s$ being the relative velocity of the fluid with respect to the solid motion, and the backward Piola transformation of \mathbf{q} , $\mathbf{Q} = J \mathbf{F}^{-1} \mathbf{q}$, which is referred to as the *material* filtration velocity.

2.2 Directional averages

At the scale of a single fibre, the fibre appears as a curved cylinder whose length is much larger than the diameter of the cross section. This allows to model the fibre as a curve. Furthermore, in a sufficiently small neighbourhood of a given point $X \in \mathcal{B}$, a fibre can be approximated by its tangent line [15], which defines the local direction of fibre alignment. Such direction can be associated with a unit vector, \mathbf{M}_X , emanating from X . Since the orientation of the fibres is assumed to be statistical at each point, we need to define the probability density that a fibre passing by X is oriented along a given direction. To this end, we introduce the set of all unit vectors of $T_X\mathcal{B}$, i.e., $\mathbb{S}_X^2\mathcal{B} = \{\mathbf{M}_X \in T_X\mathcal{B} : \|\mathbf{M}_X\| = 1\}$, and the function $\Psi_X : \mathbb{S}_X^2\mathcal{B} \rightarrow \mathbb{R}_0^+$ such that, for a given $\mathbf{M}_X \in \mathbb{S}_X^2\mathcal{B}$, $\Psi_X(\mathbf{M}_X)$ is the probability density that a (rectified) fibre passing from X is locally aligned along \mathbf{M}_X . Since Ψ_X is assumed to be a continuous probability density, it has to be normalised.

Given a physical property (e.g., a scalar one) depending on the direction of the fibres at X , and expressed thus as $\mathfrak{F}_X : \mathbb{S}_X^2\mathcal{B} \rightarrow \mathbb{R}$, the *directional average* of \mathfrak{F}_X is defined by (see, e.g., [16] and references therein)

$$\begin{aligned} \langle\langle \mathfrak{F}_X \rangle\rangle &= \int_{\mathbb{S}_X^2\mathcal{B}} \mathfrak{F}_X(\mathbf{M}_X) \Psi_X(\mathbf{M}_X) \\ &= \int_0^{2\pi} \int_0^\pi \mathfrak{F}_X(\hat{\mathbf{M}}_X(\Theta, \Phi)) \Psi_X(\hat{\mathbf{M}}_X(\Theta, \Phi)) \sin(\Theta) d\Theta d\Phi, \end{aligned} \quad (2)$$

where, for $(\Theta, \Phi) \in [0, \pi] \times [0, 2\pi[$,

$$\mathbf{M}_X = \hat{\mathbf{M}}_X(\Theta, \Phi) = \sin \Theta \cos \Phi \mathbf{e}_1 + \sin \Theta \sin \Phi \mathbf{e}_2 + \cos \Theta \mathbf{e}_3, \quad (3)$$

and $\{\mathbf{e}_I\}_{I=1}^3$ is an orthonormal vector basis of $T_X\mathcal{B}$. The second equality in (2) stems from rephrasing the integral over $\mathbb{S}_X^2\mathcal{B}$ as a surface integral and expressing it in spherical coordinates, granted that each $\mathbf{M}_X \in \mathbb{S}_X^2\mathcal{B}$ corresponds univocally to a point on the surface of the unit sphere centred at X .

In this work, we assume that the matrix of the solid phase is isotropic and that a fibre aligned along \mathbf{M}_X at $X \in \mathcal{B}$ is transversely isotropic with respect to \mathbf{M}_X . Thus, \mathfrak{F}_X must satisfy the symmetry condition $\mathfrak{F}_X(\mathbf{H}\mathbf{M}_X) = \mathfrak{F}_X(\mathbf{M}_X)$, for all proper rotation tensors \mathbf{H} such that $\mathbf{H}\mathbf{M}_X = \pm\mathbf{M}_X$. If there exists a direction of symmetry for the whole tissue, i.e., if there exists \mathbf{M}_0 such that for all $X \in \mathcal{B}$, for all $\mathbf{M}_X \in \mathbb{S}_X^2\mathcal{B}$, and for every proper rotation tensor \mathbf{H}_0 with the property $\mathbf{H}_0\mathbf{M}_0 = \pm\mathbf{M}_0$, the invariance condition $\Psi_X(\mathbf{H}_0\mathbf{M}_X) = \Psi_X(\mathbf{M}_X)$ holds true, then the probability density is transversely isotropic with respect to \mathbf{M}_0 . Consequently, the directional average $\langle\langle \mathfrak{F}_X \rangle\rangle$ turns out to be transversely isotropic with respect to \mathbf{M}_0 , while $\mathfrak{F}_X(\mathbf{M}_X)$ is transversely isotropic with respect to \mathbf{M}_X . Further restrictions descend from the hypothesis that the physical quantities depending on the orientation of the fibres are invariant under the transformation $\mathbf{M}_X \mapsto -\mathbf{M}_X$, for all \mathbf{M}_X and for all $X \in \mathcal{B}$. To fulfil this property, the generic physical quantity \mathfrak{F}_X has to depend on \mathbf{M}_X through $\mathbf{A}_X = \mathbf{M}_X \otimes \mathbf{M}_X$, which is referred to as *structure tensor*,

and fulfils the identity $\mathbf{H}\mathbf{A}_X\mathbf{H}^T = \mathbf{A}_X$. Accordingly, the probability density must comply with the invariance condition $\Psi_X(\mathbf{M}_X) = \Psi_X(-\mathbf{M}_X)$.

When $\mathbf{M}_X \in \mathbb{S}_X^2\mathcal{B}$ is expressed as in (3), the transverse isotropy of Ψ_X implies that $\Psi_X(\hat{\mathbf{M}}_X(\Theta, \Phi))$ is independent of Φ , whence the possibility of introducing a function $\wp_X: [0, \pi] \rightarrow \mathbb{R}_0^+$ such that $\wp_X(\Theta) = \Psi_X(\hat{\mathbf{M}}_X(\Theta, \Phi))$, for all $\Phi \in [0, 2\pi[$. To be compatible with the restriction $\Psi_X(\mathbf{M}_X) = \Psi_X(-\mathbf{M}_X)$, \wp_X must respect the constraint $\wp_X(\Theta) = \wp_X(\pi - \Theta)$, for all $\Theta \in [0, \pi]$. This property is also satisfied by all the physical quantities studied in this work, and allows thus to determine the directional averages in (2) by computing the integrals over the hemisphere $\mathbb{S}_X^{2+}\mathcal{B} = \{\mathbf{M}_X \in \mathbb{S}_X^2\mathcal{B} \mid \mathbf{M}_X \cdot \mathbf{M}_0 \geq 0\}$, i.e.,

$$\begin{aligned} \langle \mathfrak{F}_X \rangle &= 2 \int_{\mathbb{S}_X^{2+}\mathcal{B}} \mathfrak{F}_X(\mathbf{M}_X) \Psi_X(\mathbf{M}_X) \\ &= \int_0^{2\pi} \int_0^{\pi/2} \mathfrak{F}_X(\hat{\mathbf{M}}_X(\Theta, \Phi)) \bar{\wp}_X(\Theta) \sin(\Theta) d\Theta d\Phi, \end{aligned} \quad (4)$$

where $\bar{\wp}_X: [0, \pi/2] \rightarrow \mathbb{R}_0^+$ is a re-definition of \wp_X . Very often, the von Mises probability density is used when spherical data are concerned [8, 10, 38]. Here, however, for our purposes, we employ the pseudo-Gaussian density

$$\bar{\wp}_X(\Theta) = \frac{\gamma_X(\Theta)}{2\pi \int_0^{\pi/2} \gamma_X(\Theta') \sin(\Theta') d\Theta'}, \quad (5a)$$

$$\gamma_X(\Theta) = \exp\left(-\frac{[\Theta - Q(X)]^2}{2[\omega(X)]^2}\right), \quad (5b)$$

where $Q(X)$ and $[\omega(X)]^2$ represent the mean angle and variance of the probability density, respectively. The choice of the pseudo-Gaussian distribution is corroborated by the fact that it modelled satisfactorily the orientation of the collagen fibres in articular cartilage [9], as determined in the X-ray diffraction experiments carried out in [18].

With a slight abuse of terminology, we call $\mathbb{S}_X^2\mathcal{B}$ *unit sphere* attached at X and, in analogy with the definition of $T\mathcal{B}$, we call *bundle of unit spheres* the set $\mathbb{S}^2\mathcal{B} = \sqcup_{X \in \mathcal{B}} \mathbb{S}_X^2\mathcal{B}$. When the point $X \in \mathcal{B}$ is not specified, we adopt the notation $\Psi: \mathbb{S}^2\mathcal{B} \rightarrow \mathbb{R}_0^+$ and $\mathfrak{F}: \mathbb{S}^2\mathcal{B} \rightarrow \mathbb{R}$, thereby defining both Ψ and \mathfrak{F} over $\mathbb{S}^2\mathcal{B}$. In this case, we introduce the vector field $\mathbf{M}: \mathcal{B} \rightarrow \mathbb{S}^2\mathcal{B}$ such that $\mathbf{M}(X) = \mathbf{M}_X \in \mathbb{S}_X^2\mathcal{B} \subset \mathbb{S}^2\mathcal{B}$, and we set $\Psi(\mathbf{M}(X)) = \Psi_X(\mathbf{M}_X)$ and $\mathfrak{F}(\mathbf{M}(X)) = \mathfrak{F}_X(\mathbf{M}_X)$. Hence, we denote the directional average of \mathfrak{F} by

$$\langle \mathfrak{F} \rangle := \int_{\mathbb{S}^2\mathcal{B}} \Psi(\mathbf{M}) \mathfrak{F}(\mathbf{M}), \quad (6)$$

with the understanding that, when $\langle \mathfrak{F} \rangle$ is evaluated at $X \in \mathcal{B}$, one obtains $\langle \mathfrak{F} \rangle(X) = \langle \mathfrak{F}_X \rangle$. Sometimes, since \mathfrak{F} depends on the fibre orientation through the structure tensor, we also use the notation $\langle \mathfrak{F}(\mathbf{A}) \rangle = \langle \mathfrak{F} \rangle$.

2.3 Dynamics

From this point onwards, we employ the symbols “Grad” and “Div” for the gradient and divergence operators in the reference configuration (or, more generally, the body manifold) \mathcal{B} , and the symbols “grad” and “div” for the gradient and divergence operators in the physical space \mathcal{S} . This notation is standard in modern Continuum Mechanics (e.g. [41]) and allows us to be consistent with our previous works, to which we constantly make reference (for some remarks about the notation used in this work, see Appendix A).

We formulate the dynamics of the considered system under the hypothesis that its constituents (e.g., matrix, fibres, and fluid) have constant mass densities, and no mass exchange processes occur. These assumptions permit to write the mass balance laws of matrix and fibres as $\dot{\Phi}_{0s} = 0$ and $\dot{\Phi}_{1s} = 0$, where the material volumetric fractions $\Phi_{0s} = J\phi_{0s}$ and $\Phi_{1s} = J\phi_{1s}$ are the backward Piola transformations of the spatial volumetric fractions ϕ_{0s} and ϕ_{1s} , respectively. Clearly, Φ_{0s} and Φ_{1s} are independent of time, but they may depend on material points. Moreover, in the material formalism, the balance law of the fluid phase reads

$$\dot{J} + \text{Div } \mathbf{Q} = 0. \quad (7)$$

We recall that our formulation assumes that matrix and fibres undergo the same motion.

Hereafter, we consider the limit of negligible inertial forces and the action of no body forces. Moreover, we assume the validity of Darcy’s law. Consistently with this assumption, the Cauchy stress tensor of the fluid phase reduces to $\boldsymbol{\sigma}_f = -\phi_f p \mathbf{g}^{-1}$, where p is called *pore pressure*, and the filtration velocity \mathbf{q} is expressed as $\mathbf{q} = -\mathbf{k} \text{grad } p$, with \mathbf{k} being the tissue’s permeability tensor. Analogously, the material filtration velocity is given by $\mathbf{Q} = -\mathbf{K} \text{Grad } p$, where $\mathbf{K} = J\mathbf{F}^{-1}\mathbf{k}\mathbf{F}^{-T}$ is the material permeability tensor.

The employment of Darcy’s law allows to consider only one momentum balance law for the medium as a whole. By introducing the Cauchy stress tensor of the solid phase, $\boldsymbol{\sigma}_s = -\phi_s p \mathbf{g}^{-1} + \boldsymbol{\sigma}_{sc}$, where $\boldsymbol{\sigma}_{sc}$ is said to be the *constitutive part* of $\boldsymbol{\sigma}_s$, and since the system is assumed to be closed with respect to momentum, the momentum balance law reads $\text{div } \boldsymbol{\sigma} = \mathbf{0}$, where $\boldsymbol{\sigma} \equiv \boldsymbol{\sigma}_f + \boldsymbol{\sigma}_s$ is the overall Cauchy stress tensor of the medium in the limit of negligibly small relative velocity $\mathbf{w} = \mathbf{v}_f - \mathbf{v}_s$. To express the balance of momentum in material formalism, we introduce the first Piola-Kirchhoff stress tensors of the fluid phase and of the solid phase, i.e., $\mathbf{P}_f = J\boldsymbol{\sigma}_f\mathbf{F}^{-T}$ and $\mathbf{P}_s = J\boldsymbol{\sigma}_s\mathbf{F}^{-T}$, respectively, and we obtain

$$\text{Div} \left(-Jp\mathbf{g}^{-1}\mathbf{F}^{-T} + \mathbf{P}_{sc} \right) = \mathbf{0}, \quad (8)$$

where the term between parentheses is the overall first Piola-Kirchhoff stress tensor of the system, i.e., the sum of \mathbf{P}_f and \mathbf{P}_s , and $\mathbf{P}_{sc} = J\boldsymbol{\sigma}_{sc}\mathbf{F}^{-T}$ is the constitutive part of \mathbf{P}_s .

Equations (7) and (8) model the deformation of hydrated soft tissues and the flow of their interstitial fluids, but they cannot describe the dynamics of the internal structure of such tissues. These dynamics, indeed, involve also other processes, which generally occur at different time and length scales, and have distinct biological features. Typical examples of these processes are given by growth, resorption, damage, and reorientation of the network of collagen fibres. A more detailed tissue model should thus consider all these processes and the interactions among them. Nevertheless, we assume here that it is possible to select a modelling range in which one of the aforementioned phenomena can be studied independently of the other ones, at least conceptually [39]. On the basis of this assumption, we propose a theoretical setting in which, besides deformation and fluid flow, we account for the reorientation of fibres in a fibre-reinforced tissue. Moreover, although we present a mathematical model originally conceived for articular cartilage, our results can be extended also to other fibre-reinforced tissues.

We claim that remodelling manifests itself through an evolution in time of the mean angle, Q , which has been introduced in the probability density defined in (5a) and (5b). Thus, we call Q *remodelling variable* from here on. Also ω could be taken as a remodelling variable. However, as done in [39], we prefer here to keep the theory as simple as possible. Thus, we choose ω as a prescribed function of the material points. The remodelling angle Q , instead, evolves starting either from a histological distribution or from a “test” distribution. In the latter case, one aims to see under which conditions the system remodels towards histological patterns. To emphasise that the probability density depends on time through Q (which is now viewed as a function of time and material points), we re-define γ_X and $\bar{\rho}_X$ [cf. (5a) and (5b)] as follows:

$$\bar{\rho}_X(\Theta) = \hat{\rho}(\Theta, X, t) = \frac{\gamma_X(\Theta, X, t)}{2\pi \int_0^{\pi/2} \gamma_X(\Theta', X, t) \sin(\Theta') d\Theta'}, \quad (9a)$$

$$\gamma_X(\Theta) = \hat{\gamma}(\Theta, X, t) = \exp\left(-\frac{[\Theta - Q(X, t)]^2}{2[\omega(X)]^2}\right). \quad (9b)$$

Equations (9a) and (9b) imply that also the probability density Ψ_X depends on time through Q and, consequently, the directional average $\langle\langle \mathfrak{F}_X \rangle\rangle$ must be regarded as a functional of the remodelling variable, Q . To highlight this dependence, we use the notation $\langle\langle \mathfrak{F}_X \rangle\rangle \equiv \langle\langle \mathfrak{F}_X \rangle\rangle(Q)$ from here on.

We remark that the picture of remodelling discussed here and in [22, 39] features some similarities with the framework presented Baaijens et al. [42], of which we were unfortunately unaware at the time we wrote the papers [22, 39]. Thus, we take the occasion of this work to state that a description of remodelling based on the evolution of the mean angle characterising the fibres’ pseudo-Gaussian probability density can also be found in [42] (cf. Equation (20) of [42]). However, the approach proposed in [22], subsequently developed in [39], and further extended in our work, differs from the one presented in [42] due to the different definition of the generalised forces that drive remodelling,

and due to the different methodological framework within which the theory of remodelling is established.

Following the theory outlined in [19], and subsequently adopted in [27, 23], we embrace the line thought according to which the structural evolution of a tissue calls for the introduction of suitable “structural descriptors”. These add themselves to the descriptors associated with the standard kinematics of a tissue, namely the velocities of the solid and the fluid phase (or, alternatively, the velocity of the solid phase, \mathbf{v}_s , and the velocity \mathbf{w} of the fluid relative to the solid). Within the present framework, we identify the tissue’s structural descriptor with the time derivative of the remodelling variable, \dot{Q} , and we call “remodelling forces” the mechanical entities power-conjugate to \dot{Q} [19, 27, 23]. We distinguish these forces into “internal” and “external”, we denote them \mathcal{R}_{int} and \mathcal{R}_{ext} , respectively, and we postulate the force balance [27, 22, 23]

$$\mathcal{R}_{\text{int}} = \mathcal{R}_{\text{ext}}. \quad (10)$$

In conclusion, our theory of remodelling is based on the set of equations (7), (8) and (10), along with (the material counterpart of) Darcy’s law $\mathbf{Q} = -\mathbf{K} \text{Grad } p$. We emphasise that we are not regarding Q as an internal variable. Rather, Q is a kinematic variable, having the same “dignity” as the solid phase motion χ , and being determined by solving the balance law (10) associated with it.

Remodelling and deformation couple with each other and, together with fluid flow, drive the overall evolution of the tissue. Such evolution is known after the set of equations (7), (8), and (10) is solved, and the motion χ , pressure p , and remodelling variable Q are determined. To this end, the *remodelling equation* (10) must be rewritten in such a way that it is explicitly solvable for Q . This, in fact, requires to find admissible constitutive laws for the generalised force \mathcal{R}_{int} . To check for thermodynamic admissibility, we exploit the dissipation inequality.

We remark that, since our remodelling variable is a scalar parameter, non-planar remodelling directions cannot be taken into account by our theory. Our choice, however, is meant to keep our model as simple as possible. The model, indeed, can be generalised by introducing two independent remodelling angles, having the meaning of co-latitude and longitude, respectively, and being sufficient to determine univocally the unit vector along which the fibres tend to be aligned.

3 Constitutive theory

To close the mathematical model, constitutive laws for \mathbf{K} and \mathbf{P}_{sc} must be supplied. Moreover, whereas the functional form of \mathcal{R}_{ext} has to be prescribed from the outset, \mathcal{R}_{int} must be determined constitutively. In order to do that, a suitable constitutive theory has to be formulated.

3.1 Permeability tensor

Following [43], the permeability tensor of a fibre-reinforced porous medium can be determined by invoking the Representation Theorem for functions valued in the space of symmetric second-order tensors [44, 45]. Here, we consider the results presented in [43] for the case of a medium exhibiting transverse isotropy with respect to \mathbf{M} and, in particular, for the permeability tensor associated with the single fibre, we take the simple expression

$$\mathbf{k}_{\text{fibre}} = k_0 \mathbf{g}^{-1} + J^{-2} k_0 \mathbf{a}, \quad (11)$$

where k_0 is the scalar permeability of the matrix, and \mathbf{a} is defined by

$$\mathbf{a} = \frac{1}{I_4} \mathbf{F} \mathbf{A} \mathbf{F}^T, \quad (12)$$

where $I_4 \equiv I_4(\mathbf{C}, \mathbf{A}) = \mathbf{C} : \mathbf{A}$ is the fourth invariant of \mathbf{C} . Note that the original model of Ateshian and Weiss [43] is expressed in terms of the push-forward $\mathbf{F} \mathbf{A} \mathbf{F}^T$ of the material structure tensor \mathbf{A} , whereas (11) features the normalised spatial structure tensor \mathbf{a} . In (11), we assume for k_0 the Holmes and Mow constitutive law [46]

$$k_0 = \hat{k}_0(J) = k_{0R} \left[\frac{J - \Phi_s}{1 - \Phi_s} \right]^{\kappa_0} \exp\left(\frac{1}{2} m_0 [J^2 - 1]\right), \quad (13)$$

where k_{0R} , κ_0 , and m_0 are model parameters. Note that $\mathbf{k}_{\text{fibre}}$ is a function of \mathbf{F} and \mathbf{A} , i.e., $\mathbf{k}_{\text{fibre}} = \hat{\mathbf{k}}_{\text{fibre}}(\mathbf{F}, \mathbf{A})$. Moreover, the spatial permeability of the tissue, \mathbf{k} , is obtained by computing the directional average of $\mathbf{k}_{\text{fibre}}$, i.e.,

$$\begin{aligned} \mathbf{k} &= \hat{\mathbf{k}}(\mathbf{F}, Q) = \langle \hat{\mathbf{k}}_{\text{fibre}}(\mathbf{F}, \mathbf{A}) \rangle(Q) \\ &= \hat{k}_0(J) \mathbf{g}^{-1} + J^{-2} \hat{k}_0(J) \mathbf{F} \hat{\mathbf{Z}}(\mathbf{C}, Q) \mathbf{F}^T, \end{aligned} \quad (14)$$

where we introduced the notation

$$\hat{\mathbf{Z}}(\mathbf{C}, Q) = \left\langle \frac{\mathbf{A}}{I_4(\mathbf{C}, \mathbf{A})} \right\rangle(Q). \quad (15)$$

Finally, the material permeability $\mathbf{K} = J \mathbf{F}^{-1} \mathbf{k} \mathbf{F}^{-T}$ takes on the form

$$\mathbf{K} = \hat{\mathbf{K}}(\mathbf{C}, Q) = J \hat{k}_0(J) \mathbf{C}^{-1} + J^{-1} \hat{k}_0(J) \hat{\mathbf{Z}}(\mathbf{C}, Q). \quad (16)$$

3.2 Free energy density

Our constitutive theory relies on the assumption that the tissue can be associated with a free energy density consisting of the sum of two contributions, i.e.,

$$W := W_{\text{std}} + W_{\text{rem}}. \quad (17)$$

The first summand, W_{std} , is the strain energy density introduced in [16] to model a transversely isotropic biphasic medium with statistical orientation of the fibres. The subscript “std” means that it is regarded as *standard* in the present framework. We write explicitly the expression of W_{std} with the purpose of highlighting its dependence on the remodelling variable:

$$W_{\text{std}} = \hat{W}_{\text{std}}(\mathbf{C}, Q) = \Phi_s \hat{U}(J(\mathbf{C})) + \Phi_{0s} \hat{W}_0(\mathbf{C}) + \Phi_{1s} \hat{W}_e(\mathbf{C}, Q). \quad (18)$$

Here, Φ_{0s} and Φ_{1s} are the volumetric fractions of matrix and fibres in the reference configuration, respectively, while $\Phi_s = \Phi_{0s} + \Phi_{1s}$ is the volumetric fraction of the solid phase as a whole in the same configuration. The term $\hat{U}(J(\mathbf{C}))$ is a penalty enforcing the intrinsic incompressibility of the solid phase at compaction [16], $\hat{W}_0(\mathbf{C})$ is the isotropic strain energy density of the matrix, and $\hat{W}_e(\mathbf{C}, Q)$ is referred to as “ensemble potential” [14], and constitutes the anisotropic contribution to W_{std} , i.e.,

$$\hat{W}_e(\mathbf{C}, Q) = \hat{W}_{1i}(\mathbf{C}) + \langle \hat{W}_{1a}(\mathbf{C}, \mathbf{A}) \rangle(Q). \quad (19)$$

The energy densities $\hat{U}(J(\mathbf{C}))$, $\hat{W}_0(\mathbf{C})$, $\hat{W}_{1i}(\mathbf{C})$, and $\hat{W}_{1a}(\mathbf{C}, \mathbf{A})$ are given by

$$\hat{U}(J) = \alpha_0 \mathcal{H}(J_{\text{cr}} - J) [J - J_{\text{cr}}]^{2q} [J - \Phi_s]^{-r}, \quad (20a)$$

$$\hat{W}_0(\mathbf{C}) = \hat{W}_{1i}(\mathbf{C}) = \alpha_0 \frac{\exp(\alpha_1 [I_1 - 3] + \alpha_2 [I_2 - 3])}{[I_3]^{\alpha_3}}, \quad (20b)$$

$$\hat{W}_{1a}(\mathbf{C}, \mathbf{A}) = \mathcal{H}(I_4 - 1) \frac{1}{2} c [I_4 - 1]^2, \quad (20c)$$

where \mathcal{H} is the Heaviside function (here, $\mathcal{H}(s) = 0$ for all $s \leq 0$, and $\mathcal{H}(s) = 1$ for all $s > 0$) [38], and we used the short-hand notation $J = J(\mathbf{F}) = \det \mathbf{F}$ for the volume ratio, $I_1 = I_1(\mathbf{C}) = \text{tr}(\mathbf{C})$, $I_2 = I_2(\mathbf{C}) = \frac{1}{2} \{[\text{tr}(\mathbf{C})]^2 - \text{tr}(\mathbf{C}^2)\}$, $I_3 = I_3(\mathbf{C}) = \det \mathbf{C}$ for the three principal invariants of \mathbf{C} , and $I_4 = I_4(\mathbf{C}, \mathbf{A}) = \mathbf{C} : \mathbf{A}$ for the fourth invariant of \mathbf{C} . In (20a), $J_{\text{cr}} \in]\Phi_s, 1]$ is a “critical” value of J below which the penalty term is switched on to prevent J from approaching the lower physical bound Φ_s , while $q \geq 2$ and $r \in]0, 1]$ are model parameters. In (20b) and (20c), α_0 , α_1 , α_2 , α_3 , and c are model parameters and, in particular, α_0 and c have the same physical units as the strain energy density and determine the energy scales characterising the isotropic and anisotropic contributions of \hat{W}_{std} . The term $\hat{W}_{1i}(\mathbf{C})$ is the isotropic contribution of the fibres to the tissue’s overall strain energy density, and $\hat{W}_{1a}(\mathbf{C}, \mathbf{A})$ is the anisotropic contribution, which depends on the fibre alignment through $\mathbf{A} = \mathbf{M} \otimes \mathbf{M}$. The fact that \hat{W}_{1i} is taken here to be equal to \hat{W}_0 is just a model assumption [38]. We remark that the directional average of $\hat{W}_{1a}(\mathbf{C}, \mathbf{A})$, i.e., $\langle \hat{W}_{1a}(\mathbf{C}, \mathbf{A}) \rangle$, depends on the remodelling variable, Q , through the probability density.

The idea underlying the definition of the energy density given in (18) can be found in several works on composite materials [47–49]. In these papers, a given composite material is modelled within the theory of linear elasticity, and the elasticity tensor of the material is written as the weighted sum of the elasticity tensors of its constituents, each multiplied by the corresponding

volumetric fraction. In this sum, however, the weights depend on the strain concentration tensor [49, 50] and, thus, on Eshelby's fourth-order tensor [51]. In the non-linear framework, instead, the Eshelby-like formulation is not directly applicable and, if the constituents of a composite material are assumed to be hyperelastic, the elastic potential of the composite as a whole can be constructed by weighing the elastic potentials of the constituents. In some cases, e.g. [2, 27], the elastic potentials contain the volumetric fractions in their own definition, whereas we put them in evidence in our formulation. In (18), indeed, apart from $\hat{\Phi}_s \hat{U}(J(\mathbf{C}))$, W_{std} is the weighted sum of one contribution due to the matrix and one due to the fibres, the weights being the volumetric fractions $\hat{\Phi}_{0s}$ and $\hat{\Phi}_{1s}$.

Moreover, in the present work, the isotropic energy densities $\hat{W}_0(\mathbf{C})$ and $\hat{W}_{1i}(\mathbf{C})$ depend on I_3 , thereby describing a compressible behaviour of the modelled material, while the anisotropic contribution, $\hat{W}_{1a}(\mathbf{C}, \mathbf{A})$, is assumed to depend on \mathbf{C} through I_4 only. In fact, the tissue described by (18), (19), and (20a)–(20c) is compressible and anisotropic, which requires its elastic energy density to depend both on I_3 and —at least— on I_4 . However, the way in which compressibility and anisotropy are modelled is not unique and, in this respect, the additive decomposition of the energy density performed in (18) and (19), in which the compressible effects are attributed solely to the isotropic terms, is only one among other possible choices. To give an example, indeed, in the work by Almeida and Spilker [52] on articular cartilage, the elastic energy density is anisotropic and compressible, but the decomposition presented in (18) and (19) was not enforced. We would like to emphasise, however, that decompositions of this kind are rather customary in the study of fibre-reinforced hyperelastic materials (see e.g. [2, 27] for the case of blood vessels). Moreover, strictly speaking, since I_4 can be further decomposed multiplicatively as $I_4 = I_3^{1/3} \bar{I}_4$, with $\bar{I}_4 = \bar{\mathbf{C}} : \mathbf{A}$ and $\det \bar{\mathbf{C}} = 1$, the anisotropic part of the energy density still models a compressible material.

The second summand of (17), W_{rem} , is the part of the free energy density that is directly related to remodelling. This term is the main novelty of our constitutive theory, which is based on the requirement that W_{rem} admits the representation

$$W_{\text{rem}} = \hat{W}_{\text{rem}}(\mathbf{C}, Q, \text{Grad } Q) = \hat{W}_{\text{str}}(\mathbf{C}, Q) + \hat{W}_{\text{grad}}(\mathbf{C}, \text{Grad } Q). \quad (21)$$

The energy densities $\hat{W}_{\text{grad}}(\mathbf{C}, \text{Grad } Q)$ and $\hat{W}_{\text{str}}(\mathbf{C}, Q)$ are given by

$$W_{\text{grad}} = \hat{W}_{\text{grad}}(\mathbf{C}, \text{Grad } Q) = \frac{1}{2} \hat{\mathbf{D}}(\mathbf{C}) : \text{Grad } Q \otimes \text{Grad } Q, \quad (22a)$$

$$W_{\text{str}} = \hat{W}_{\text{str}}(\mathbf{C}, Q) = \hat{\mathcal{A}}(\mathbf{C}) \hat{\mathcal{P}}(Q) \exp(\hat{\alpha}_W(\mathbf{C}) Q), \quad (22b)$$

where the subscript “grad” indicates that \hat{W}_{grad} depends on the gradient of the mean angle, while the subscript “str” means that \hat{W}_{str} is directly related to the internal structure of the tissue. The quantity $\hat{\mathbf{D}}(\mathbf{C})$ is a symmetric, positive semi-definite, second-order tensor-valued function of \mathbf{C} , $\hat{\mathcal{A}}(\mathbf{C})$ is a non-negative coefficient with physical units of energy per unit volume, $\hat{\mathcal{P}}(Q)$

is a dimensionless, non-negative function of Q , and $\hat{\alpha}_W(\mathbf{C})$ is a dimensionless, non-negative coefficient. In the absence of deformation, i.e., when \mathbf{C} equals the material metric tensor \mathbf{G} (which serves here as the “covariant identity tensor”), we set $\hat{\mathbf{D}}(\mathbf{G}) = \mathbf{D}_0$, $\hat{\mathcal{A}}(\mathbf{C}) = \mathcal{A}_0 \geq 0$, and $\hat{\alpha}_W(\mathbf{G}) = 0$.

The term $\hat{W}_{\text{grad}}(\mathbf{C}, \text{Grad } Q)$ is introduced to explicitly account for the spatial resolution of the remodelling variable, Q . Physically, it represents the contribution to the overall energy that is set off by the first-order spatial variations of Q at each material point. To keep the proposed theory at a minimal level of complexity, we assume that $\hat{W}_{\text{grad}}(\mathbf{C}, \text{Grad } Q)$ is quadratic in $\text{Grad } Q$. As is the case for other theories based on energy densities that depend on the gradient of an angular variable (for example, the energy of the Sine-Gordon model [53]), $\hat{\mathbf{D}}(\mathbf{C})$ could be thought of as a measure of the system’s “angular stiffness per unit length”. Indeed, it determines the response of the system to the spatial variations of Q . We remark that, by its own definition, $\hat{\mathbf{D}}(\mathbf{C})$ is modulated by \mathbf{C} , which means that, in general, the tissue’s angular stiffness varies with the deformation. If, on the one hand, the evolution of the remodelling angle Q influences the elastic response of the tissue through the term $\hat{W}_e(\mathbf{C}, Q)$ [see Equation (18)], the tensor $\hat{\mathbf{D}}(\mathbf{C})$ couples the global changes of shape of the tissue with its structural transformations, which are represented by the variations of Q in time and space.

Before providing a term-by-term explanation of $\hat{W}_{\text{str}}(\mathbf{C}, Q)$ [see (22b)], we discuss the logical steps that lead to its functional form. First, we remark that, since in this work the kinematics of the tissue is described by χ and Q , the configuration attained by the tissue at time t is determined by both $\chi(X, t)$ and $Q(X, t)$, for all $X \in \mathcal{B}$. Second, we claim that each such configuration can be associated with an energy that depends on the deformation *and* the distribution of the fibre mean angle throughout the tissue. Third, by exploiting the fact that the deformation and the mean angle are independent on each other, we also claim that there exist distributions of the fibre mean angle that endow the tissue with non-trivial energies even in the absence of deformation. Indeed, even though W_{std} reduces to the unessential constant $\hat{W}_{\text{std}}(\mathbf{G}, Q) \equiv \hat{W}_{\text{std}}^{(0)}(Q) = \alpha_0$ in such cases [see (18) and (20a)–(20c)], W_{str} and W_{grad} become

$$\hat{W}_{\text{str}}(\mathbf{G}, Q) \equiv \hat{W}_{\text{str}}^{(0)}(Q) = \mathcal{A}_0 \hat{\mathcal{P}}(Q), \quad (23a)$$

$$\hat{W}_{\text{grad}}(\mathbf{G}, \text{Grad } Q) \equiv \hat{W}_{\text{grad}}^{(0)}(\text{Grad } Q) = \frac{1}{2} \mathbf{D}_0 : \text{Grad } Q \otimes \text{Grad } Q, \quad (23b)$$

thereby yielding

$$\begin{aligned} W_{\text{rem}} &\equiv \hat{W}_{\text{rem}}^{(0)}(Q, \text{Grad } Q) = \hat{W}_{\text{str}}^{(0)}(Q) + \hat{W}_{\text{grad}}^{(0)}(\text{Grad } Q), \\ &= \mathcal{A}_0 \hat{\mathcal{P}}(Q) + \frac{1}{2} \mathbf{D}_0 : \text{Grad } Q \otimes \text{Grad } Q, \end{aligned} \quad (24a)$$

$$\begin{aligned} W &\equiv \hat{W}_{\text{std}}^{(0)}(Q) + \hat{W}_{\text{rem}}^{(0)}(Q, \text{Grad } Q) \\ &= \alpha_0 + \hat{W}_{\text{rem}}^{(0)}(Q, \text{Grad } Q). \end{aligned} \quad (24b)$$

If \mathbf{D}_0 is positive definite and \mathcal{A}_0 strictly positive, $\hat{W}_{\text{rem}}^{(0)}(Q, \text{Grad } Q)$ is zero only for those distributions of the fibre mean angle that are spatially uniform

and solutions of $\hat{\mathcal{P}}(Q) = 0$. In the jargon of [53], a time-independent field Q satisfying these conditions is said to be a “*classical vacuum*” configuration for $\hat{W}_{\text{rem}}^{(0)}(Q, \text{Grad } Q)$, since it determines the lowest energy of the system under study (zero, in the considered case). In general, however, when Q is not a vacuum configuration, $\hat{W}_{\text{rem}}^{(0)}(Q, \text{Grad } Q)$ is greater than zero and consists of the contribution due to the spatial variability of Q , i.e., $\hat{W}_{\text{grad}}^{(0)}(\text{Grad } Q)$, and of the contribution due to the potential energy density associated with Q , i.e., $\hat{W}_{\text{str}}^{(0)}(\text{Grad } Q)$. Thus, up to α_0 , $\hat{W}_{\text{rem}}^{(0)}(Q, \text{Grad } Q)$ is the energy density that characterises the tissue for a given Q , and the integral

$$\begin{aligned} \mathcal{W}_{\text{rem}}^{(0)}[Q] &= \int_{\mathcal{B}} \hat{W}_{\text{rem}}^{(0)}(Q, \text{Grad } Q) \\ &= \int_{\mathcal{B}} \left\{ \mathcal{A}_0 \hat{\mathcal{P}}(Q) + \frac{1}{2} \mathbf{D}_0 : \text{Grad } Q \otimes \text{Grad } Q \right\} \end{aligned} \quad (25)$$

is the tissue’s energy corresponding to Q . In conclusion, and consistently with what we claimed above, our interpretation of (25) is that any conformation of the tissue’s internal structure, which is described by selecting an appropriate distribution of the fibre mean angle, yields an energy. This energy, in turn, is nonzero as long as the distribution of the fibre mean angle is not a vacuum configuration.

As explained in Section 4.1, we assume that the information on the internal structure of the tissue is supplied by the histological pattern with which the fibres are oriented in the undeformed tissue and, thus, by the distribution of the fibre mean angle associated with it. Such distribution, denoted by Q_{h} , can be determined experimentally. In fact, as shown in Fig. 2, it features a sigmoidal shape and takes on the values $Q_0 = 0 \text{ rad}$ and $Q_1 = \pi/2 \text{ rad}$ at the lower and upper boundary, respectively, of the cylindrical samples of tissue adopted in the study [54].

Although a functional form for Q_{h} can be obtained by fitting experimental data [54], we follow here a rather different approach. First, since the sigmoidal profile of Q_{h} goes from Q_0 to Q_1 , we invoke a formal analogy with the theory of phase transitions, and we claim that $\hat{W}_{\text{str}}^{(0)}(Q)$ should be a double-well energy density of the Allen-Cahn type, with $Q_0 = 0 \text{ rad}$ and $Q_1 = \pi/2 \text{ rad}$ being its global minimum configurations. Thus, with reference to the undeformed configuration of the tissue, we set

$$\hat{W}_{\text{str}}^{(0)}(Q) \equiv \hat{W}_{\text{AC}}^{(0)}(Q) = \frac{\mathcal{A}_0}{(\pi/4)^4} Q^2 \left(Q - \frac{\pi}{2} \right)^2, \quad (26)$$

where $\hat{W}_{\text{AC}}^{(0)}(Q)$ is the Allen-Cahn energy density [26]. We notice that Equations (23a) and (26) allow to identify $\hat{\mathcal{P}}(Q)$ with

$$\hat{\mathcal{P}}(Q) = \frac{1}{(\pi/4)^4} Q^2 \left(Q - \frac{\pi}{2} \right)^2, \quad (27)$$

i.e., with a polynomial of degree four in Q that vanishes for $Q_0 = 0$ rad and $Q_1 = \pi/2$ rad, and whose global maximum over $[0, \pi/2]$ is attained at $Q_{\max} = \pi/4$ rad.

We emphasise that the zeroes of $\hat{\mathcal{P}}(Q)$ are the vacuum configurations of the Allen-Cahn energy density defined in Equation (26), for which it holds, thus, $\hat{W}_{\text{AC}}^{(0)}(Q_0) = \hat{W}_{\text{AC}}^{(0)}(Q_1) = 0$. Accordingly, the sigmoidal profile of Q_h describes a transition from Q_0 to Q_1 , and the quantity \mathcal{A}_0 , which is equal to the global maximum of $\hat{W}_{\text{AC}}^{(0)}(Q)$, defines the height of the energy barrier separating Q_0 from Q_1 .

When the deformation is considered, the height of the energy barrier, \mathcal{A}_0 , is generally allowed to be modulated by the deformation, and becomes $\hat{\mathcal{A}}(\mathbf{C})$. Moreover, whereas $\hat{W}_{\text{AC}}^{(0)}(Q)$ is symmetric with respect to $Q = \pi/4$ rad, the coefficient $\hat{\alpha}_W(\mathbf{C})$ destroys this symmetry for $\mathbf{C} \neq \mathbf{G}$. In conclusion, by using the expression of $\hat{\mathcal{P}}(Q)$ given in (27), we can interpret the structural part of the energy density, $\hat{W}_{\text{str}}(\mathbf{C}, Q)$, as a generalised, deformation-dependent energy density of the Allen-Cahn type, i.e.,

$$\hat{W}_{\text{AC}}(\mathbf{C}, Q) \equiv \hat{W}_{\text{str}}(\mathbf{C}, Q) = \hat{\mathcal{A}}(\mathbf{C}) \hat{\mathcal{P}}(Q) \exp(\hat{\alpha}_W(\mathbf{C})Q). \quad (28)$$

Although all the results presented in this work have been obtained by employing $\hat{W}_{\text{AC}}^{(0)}(Q)$ and $\hat{W}_{\text{AC}}(\mathbf{C}, Q)$, these energy densities may have to be replaced with more appropriate constitutive choices in the case of different histological distributions of the mean angle, or for tissues other than articular cartilage. However, if the spatial resolution of the mean angle has to be explicitly taken into account, a “gradient-part” of the remodelling energy, like the one defined in (22a), may still be employed.

Once the Allen-Cahn energy density (28) is introduced, we claim that Q_h can be determined as the solution of a variational problem. To this end, indeed, we require that the first-order variation of the functional $\mathcal{W}_{\text{rem}}^{(0)}$, defined in (25), is zero for arbitrary variations of Q_h .

In Section 4.1 it will be shown that Q_h is computed by solving a differential equation equipped with the Dirichlet boundary conditions $Q_h(X) = Q_0$, for all $X \in (\partial\mathcal{B})_{\text{L}}$, and $Q_h(X) = Q_1$, for all $X \in (\partial\mathcal{B})_{\text{U}}$, where $(\partial\mathcal{B})_{\text{L}}$ and $(\partial\mathcal{B})_{\text{U}}$ denote the lower and upper boundaries of \mathcal{B} , respectively. In this case, the magnitude of \mathbf{D}_0 influences the tendency of the fibre mean angle to become a straight line connecting Q_0 with Q_1 . This trend, in fact, is obtained in the limit in which the magnitude of \mathbf{D}_0 goes towards infinity. On the other hand, if the boundary data are changed in such a way that one of the two Dirichlet conditions is replaced by a homogeneous Neumann condition, then the magnitude of \mathbf{D}_0 measures the tendency of Q_h to distribute itself uniformly throughout the sample. When this is the case, indeed, the uniformity of Q_h increases with the magnitude of \mathbf{D}_0 . Finally, when the deformation is considered, and the evolution in time of the fibre mean angle, Q , is studied, $\hat{\mathbf{D}}(\mathbf{C})$ influences the rate at which Q approaches a stationary solution.

3.3 Dissipation Inequality

In the present context, the dissipation inequality can be cast in the form [22] (see Appendix B for details)

$$\mathfrak{D} = \mathfrak{D}_I + \mathfrak{D}_{II} + \mathfrak{D}_{III} + \mathfrak{D}_{IV} \geq 0, \quad (29)$$

where \mathfrak{D} is the residual dissipation per unit volume of the reference configuration, and the summands on the right-hand-side of (29) are given by

$$\begin{aligned} \mathfrak{D}_I = & \left\{ -\mathbf{F} \left(2 \frac{\partial \hat{W}}{\partial \mathbf{C}} \right) + \mathbf{P}_s + \Phi_s p \mathbf{g}^{-1} \mathbf{F}^{-T} \right\} : \mathbf{g} \dot{\mathbf{F}} \\ & + \left\{ \mathbf{P}_f + (J - \Phi_s) p \mathbf{g}^{-1} \mathbf{F}^{-T} \right\} : \mathbf{g} \text{Grad} \mathbf{v}_f, \end{aligned} \quad (30a)$$

$$\mathfrak{D}_{II} = -J \left[\boldsymbol{\pi}_f - p \mathbf{g}^{-1} \text{grad} \phi_f \right] \cdot \mathbf{w}, \quad (30b)$$

$$\mathfrak{D}_{III} = \left\{ - \left[\frac{\partial \hat{W}}{\partial Q} - \text{Div} \left(\frac{\partial \hat{W}}{\partial \text{Grad} Q} \right) \right] + \mathcal{R}_{\text{int}} \right\} \dot{Q}, \quad (30c)$$

$$\mathfrak{D}_{IV} = \text{Div} \left[-T \bar{\boldsymbol{\Sigma}}^\eta - \frac{\partial \hat{W}}{\partial \text{Grad} Q} \dot{Q} \right]. \quad (30d)$$

Here, $\bar{\boldsymbol{\Sigma}}^\eta$ is the entropy flux vector, and \hat{W} is expressed constitutively as

$$\hat{W}(\mathbf{C}, Q, \text{Grad} Q) = \hat{W}_{\text{std}}(\mathbf{C}, Q) + \hat{W}_{\text{rem}}(\mathbf{C}, Q, \text{Grad} Q), \quad (31a)$$

$$\hat{W}_{\text{rem}}(\mathbf{C}, Q, \text{Grad} Q) = \hat{W}_{\text{AC}}(\mathbf{C}, Q) + \frac{1}{2} \hat{\mathbf{D}}(\mathbf{C}) : \text{Grad} Q \otimes \text{Grad} Q. \quad (31b)$$

Also the constitutive part of the mechanical stress depends—at least in principle—on the same list of variables. However, to account for the dissipation related to the exchange of momentum between the fluid and the solid phase (which is represented by $\mathfrak{D}_{II} \geq 0$, and leads to Darcy's law) as well as for the dissipation associated with remodelling (i.e., $\mathfrak{D}_{III} \geq 0$), the complete list of independent constitutive variables is given by \mathbf{F} , Q , $\text{Grad} Q$, \dot{Q} , and \mathbf{w} . Furthermore, we study the dissipation inequality (29) by requiring that \mathfrak{D}_I , \mathfrak{D}_{II} , \mathfrak{D}_{III} , and \mathfrak{D}_{IV} are all non-negative, one independently on the others. Within the present theoretical framework, in which the free energy density \hat{W} features the gradient of the remodelling variable among its arguments, the entropy flux vector does not necessarily reduce to the ratio between a heat flux vector and the absolute temperature [55]. Rather, $\bar{\boldsymbol{\Sigma}}^\eta$ is defined by

$$\bar{\boldsymbol{\Sigma}}^\eta = -\frac{1}{T} \frac{\partial \hat{W}}{\partial \text{Grad} Q} \dot{Q}, \quad (32)$$

thereby establishing that \mathfrak{D}_{IV} vanishes identically. Moreover, since $\dot{\mathbf{F}}$ and $\text{Grad} \mathbf{v}_f$ are not independent constitutive variables, and \mathfrak{D}_I depends linearly on them, the sums between braces in (30a) must be zero to ensure that the

inequality $\mathfrak{D}_I \geq 0$ is fulfilled for arbitrary choices of $\dot{\mathbf{F}}$ and $\text{Grad} \mathbf{v}_f$. Hence, \mathfrak{D}_I vanishes identically. This yields the conditions

$$\mathbf{P}_s = -\Phi_s p \mathbf{g}^{-1} \mathbf{F}^{-T} + \mathbf{F} \left(2 \frac{\partial \hat{W}}{\partial \mathbf{C}} \right), \quad (33a)$$

$$\mathbf{P}_f = -(J - \Phi_s) p \mathbf{g}^{-1} \mathbf{F}^{-T}, \quad (33b)$$

$$\mathbf{P} = \mathbf{P}_s + \mathbf{P}_f = -J p \mathbf{g}^{-1} \mathbf{F}^{-T} + \mathbf{F} \left(2 \frac{\partial \hat{W}}{\partial \mathbf{C}} \right), \quad (33c)$$

so that the constitutive part \mathbf{P}_{sc} of \mathbf{P}_s and \mathbf{P} is given by

$$\mathbf{P}_{sc} = \mathbf{F} \left(2 \frac{\partial \hat{W}}{\partial \mathbf{C}} \right). \quad (34)$$

Note that, if the free energy density is given as a function of \mathbf{F} , Q , and the spatial gradient of Q , i.e., as $\hat{V}(\mathbf{F}, Q, \text{grad } Q) = \hat{W}(\mathbf{C}, Q, \text{Grad } Q)$, \mathbf{P}_{sc} admits the two equivalent expressions

$$\mathbf{P}_{sc} = \mathbf{F} \left(2 \frac{\partial \hat{W}}{\partial \mathbf{C}} \right) = \mathbf{g}^{-1} \frac{\partial \hat{V}}{\partial \mathbf{F}} + \mathbf{P}_K, \quad (35a)$$

$$\mathbf{P}_K = -\mathbf{g}^{-1} \left(\text{grad } Q \otimes \frac{\partial \hat{V}}{\partial \text{grad } Q} \right) \mathbf{F}^{-T}, \quad (35b)$$

where \mathbf{P}_K is the Piola transform of the Korteweg stress tensor [55]. We emphasise that the presence of \mathbf{P}_K , which is explicit in (35a) and hidden in (34), is a consequence of the fact that our theory employs a free energy density depending on $\text{Grad } Q$.

Finally, we define the dissipative generalised forces $\boldsymbol{\pi}_{fd}$ and \mathcal{N} , i.e.,

$$\boldsymbol{\pi}_{fd} \equiv \boldsymbol{\pi}_f - p \mathbf{g}^{-1} \text{grad } \phi_f, \quad (36a)$$

$$\mathcal{N} \equiv - \left[\frac{\partial \hat{W}}{\partial Q} - \text{Div} \left(\frac{\partial \hat{W}}{\partial \text{Grad } Q} \right) \right] + \mathcal{R}_{int}, \quad (36b)$$

so that the residual dissipation reads

$$\mathfrak{D} = -J \boldsymbol{\pi}_{fd} \cdot \mathbf{w} + \mathcal{N} \dot{Q} \geq 0. \quad (37)$$

While the first term on the right-hand-side of (37) is rather standard and is assumed to lead to Darcy's law in the present framework, the term $\mathcal{N} \dot{Q}$ is “new”, in the sense that it is generated by the presence of remodelling [27, 22, 39]. Since the remodelling equation is given by $\mathcal{R}_{int} = \mathcal{R}_{ext}$, and since \mathcal{R}_{int} comprises a dissipative part, \mathcal{N} , as well as a non-dissipative part (which coincides with the terms between brackets in (36b)), we write

$$\mathcal{R}_{int} \equiv \mathcal{N} + \left[\frac{\partial \hat{W}}{\partial Q} - \text{Div} \left(\frac{\partial \hat{W}}{\partial \text{Grad } Q} \right) \right] = \mathcal{R}_{ext}. \quad (38)$$

Hence, we obtain

$$\mathcal{N} = - \left[\frac{\partial \hat{W}}{\partial Q} - \text{Div} \left(\frac{\partial \hat{W}}{\partial \text{Grad} Q} \right) \right] + \mathcal{R}_{\text{ext}}. \quad (39)$$

Following [22,39], we prescribe \mathcal{N} to be defined through a particular simple constitutive law that is linear in \dot{Q} , i.e.,

$$\mathcal{N} = \hat{\mathcal{N}}(\mathbf{C}, Q, \dot{Q}) = \hat{F}(\mathbf{C}, Q) \dot{Q}, \quad (40)$$

with $\hat{F}(\mathbf{C}, Q) \geq 0$, so that the remodelling equation becomes

$$\begin{aligned} \hat{F}(\mathbf{C}, Q) \dot{Q} &= - \left[\frac{\partial \hat{W}}{\partial Q} - \text{Div} \left(\frac{\partial \hat{W}}{\partial \text{Grad} Q} \right) \right] + \mathcal{R}_{\text{ext}} \\ &= - \left[\frac{\partial \hat{W}}{\partial Q} - \text{Div} \left(\hat{\mathbf{D}}(\mathbf{C}) \text{Grad} Q \right) \right] + \mathcal{R}_{\text{ext}}. \end{aligned} \quad (41)$$

Equation (41) is the *remodelling equation* that rules the evolution of the remodelling variable Q . With respect to other pictures of remodelling (for instance, those put forward in [27,22,23]), the theory proposed here contains the additional internal remodelling force

$$-\text{Div} \left(\frac{\partial \hat{W}}{\partial \text{Grad} Q} \right) = -\text{Div} \left(\hat{\mathbf{D}}(\mathbf{C}) \text{Grad} Q \right). \quad (42)$$

We remark that the terms in brackets in (41) are *not* the functional derivative of \hat{W}_{rem} . Indeed, also \hat{W}_{std} depends on Q and, thus, contributes to the evolution of the remodelling variable. Before going further, we mention that similar constitutive frameworks, based however on the Cahn-Hilliard model, have been proposed in studying tumours in [56–58].

3.4 Summary of the model equations and simplifying assumptions

The model equations are given by (7), (8), and (41). These have to be solved by providing boundary conditions, as well as initial conditions for χ and Q . In this work, we consider a sample of tissue of cylindrical shape in its reference configuration, \mathcal{B} . We denote by $L = 1$ mm and $R = 1.5$ mm the initial thickness and initial radius of the sample, respectively, and we write the boundary of \mathcal{B} as the disjoint union $\partial \mathcal{B} = (\partial \mathcal{B})_{\text{L}} \sqcup (\partial \mathcal{B})_{\text{U}} \sqcup (\partial \mathcal{B})_{\text{B}}$, where $(\partial \mathcal{B})_{\text{L}}$, $(\partial \mathcal{B})_{\text{U}}$, and $(\partial \mathcal{B})_{\text{B}}$ represent the lower, upper, and lateral portions of $\partial \mathcal{B}$, respectively. The sample is assumed to be transversely isotropic with respect to the direction \mathbf{M}_0 , which coincides with the geometric symmetry axis of the cylinder.

The sample is subjected to an unconfined compression test characterised by the boundary conditions (BCs)

$$\text{On } (\partial \mathcal{B})_{\text{U}}, \quad \begin{cases} \chi^3 = \mathbf{g}, \\ (-\mathbf{K} \text{Grad} p) \cdot \mathbf{N} = 0, \end{cases} \quad (43a)$$

$$\text{On } (\partial\mathcal{B})_L, \quad \begin{cases} \chi(X, t) - \chi(X, 0) = \mathbf{0}, \\ (-\mathbf{K} \text{Grad } p) \cdot \mathbf{N} = 0, \end{cases} \quad (43b)$$

$$\text{On } (\partial\mathcal{B})_B, \quad \begin{cases} (-Jp\mathbf{g}^{-1}\mathbf{F}^{-T} + \mathbf{P}_{sc}) \cdot \mathbf{N} = 0, \\ p = 0, \end{cases} \quad (43c)$$

where χ^3 is the axial component of the solid phase motion, \mathbf{N} is the field of unit normal to $\partial\mathcal{B}$, and \mathbf{g} is the compressive loading history

$$\mathbf{g}(t) = \begin{cases} L - \frac{t}{T_{\text{ramp}}} u_T, & \text{for } t \in [0, T_{\text{ramp}}], \\ L - u_T, & \text{for } t \in]T_{\text{ramp}}, T_{\text{end}}]. \end{cases} \quad (44)$$

The target displacement $u_T = 0.2 \text{ mm}$ is reached by $(\partial\mathcal{B})_U$ at $T_{\text{ramp}} = 20 \text{ s}$, and then maintained up to $T_{\text{end}} = 100 \text{ s}$. The BCs (43a) and (43b) indicate that $(\partial\mathcal{B})_U$ and $(\partial\mathcal{B})_L$ are impermeable, with $(\partial\mathcal{B})_U$ being displaced axially according to \mathbf{g} , and $(\partial\mathcal{B})_L$ being kept fixed. The BCs (43c), instead, imply that $(\partial\mathcal{B})_B$ is permeable and free of applied surface forces. A schematic description of the considered benchmark test is given in Fig. 1.

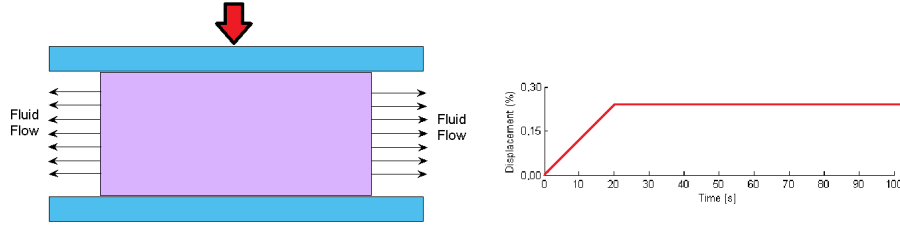


Fig. 1 Schematic description of the considered loading history. The sample is compressed along the axial direction by means of a loading ramp up to $t \leq T_{\text{ramp}} = 20 \text{ s}$, and the load is then maintained up to $T_{\text{end}} = 100 \text{ s}$.

In addition to (43a)–(43c), we also prescribe the BCs for the remodelling variable, Q , i.e.,

$$\text{On } (\partial\mathcal{B})_U, \quad Q(X, t) = \frac{\pi}{2} \text{ rad}, \quad \forall t \in]0, T_{\text{end}}], \quad (45a)$$

$$\text{On } (\partial\mathcal{B})_L, \quad Q(X, t) = 0 \text{ rad}, \quad \forall t \in]0, T_{\text{end}}], \quad (45b)$$

$$\text{On } (\partial\mathcal{B})_B, \quad (-\hat{\mathbf{D}}(\mathbf{C}) \text{Grad } Q) \cdot \mathbf{N} = 0, \quad \forall t \in]0, T_{\text{end}}] \quad (45c)$$

Finally, the initial condition on χ is expressed by requiring that the reference configuration, which coincides here with the initial one, is undeformed, while the initial condition on Q can be either obtained by fitting experimental data or computed via preliminary calculations, as explained in Section 4.1.

We remark that the boundary conditions imposed on Q are necessary to solve the partial differential equation governing its spatiotemporal evolution. Among various possible choices (i.e., boundary conditions of Dirichlet, Neumann, or mixed type), we chose Dirichlet boundary conditions because they

are easier to handle from a numerical point of view, and because they are consistent with the histological information on the pattern of fibre alignment within the tissue. Clearly, imposing these conditions on the upper and lower boundary of the sample prescribes the values of the remodelling variable on these surfaces. This, in turn, amounts to restrict the remodelling process only to the internal points of the sample, and, in the case studied in Section 4.1, guides the distribution of the fibre mean angle towards the expected result. However, this requirement seems to us weaker, and therefore more general, than prescribing the histological profile *a priori*, or selecting an *ad hoc* remodelling force \mathcal{R}_{ext} . Moreover, the use of boundary conditions of different type, and their impact on the solution describing the distribution of the fibre mean angle is part of our current investigations.

Before going further, it is important to analyse the explicit expression of $2(\partial\hat{W}/\partial\mathbf{C})$ and $\partial\hat{W}/\partial Q$. For this purpose, we invoke the constitutive laws (18)–(26), (31a) and (31b), and we enforce the simplifying assumptions $\hat{\mathcal{A}}(\mathbf{C}) = \mathcal{A}_0$, $\hat{\mathbf{D}}(\mathbf{C}) = D_0 \mathbf{G}^{-1}$ (the inverse metric \mathbf{G}^{-1} here serves as the “contravariant identity tensor”), and $\hat{I}(\mathbf{C}, Q) = I$, where \mathcal{A}_0 , D_0 , and I are assumed to be constant. Moreover, we set

$$\hat{\alpha}_W(\mathbf{C}) = \frac{1}{2}a[I_1(\bar{\mathbf{C}}) - 3]^2, \quad (46)$$

with a being a non-negative scalar constant, and $\bar{\mathbf{C}} = J^{-2/3}\mathbf{C}$. We need to clarify, however, that, since D_0 and \mathcal{A}_0 must vanish in the absence of fibres, both D_0 and \mathcal{A}_0 should be expressed by means of continuous functions of the volumetric fraction of the fibres, Φ_{1s} , that tend to zero when Φ_{1s} tends to zero. Furthermore, since Φ_{1s} is a function of the material point, D_0 and \mathcal{A}_0 should depend on the material point too. Therefore, the assumption of constant D_0 and \mathcal{A}_0 means that these coefficients correspond to averaged values of Φ_{1s} . In the cases in which this hypothesis is invalid, D_0 and \mathcal{A}_0 should be reformulated as $D_0 = \Phi_{1s}\tilde{D}_0$ and $\mathcal{A}_0 = \Phi_{1s}\tilde{\mathcal{A}}_0$, where $\tilde{D}_0 \geq 0$ and $\tilde{\mathcal{A}}_0 \geq 0$ may also depend on the material point, in general.

The assumptions done so far imply that the free energy density used for simulations is given by

$$\hat{W}(\mathbf{C}, Q, \text{Grad}Q) = \hat{W}_{\text{std}}(\mathbf{C}, Q) + \hat{W}_{\text{rem}}(\mathbf{C}, Q, \text{Grad}Q), \quad (47a)$$

$$\hat{W}_{\text{rem}}(\mathbf{C}, Q, \text{Grad}Q) = \hat{W}_{\text{AC}}(\mathbf{C}, Q) + \frac{1}{2}D_0\|\text{Grad}Q\|^2, \quad (47b)$$

$$\hat{W}_{\text{AC}}(\mathbf{C}, Q) = \mathcal{A}_0\hat{\mathcal{P}}(Q)\exp(\hat{\alpha}_W(\mathbf{C})Q), \quad (47c)$$

with $\hat{\alpha}_W(\mathbf{C})$ being defined in (46). Hence, we find

$$\begin{aligned} \hat{\mathbf{P}}_{\text{sc}} &= \mathbf{F} \left(2 \frac{\partial \hat{W}}{\partial \mathbf{C}} \right) = \mathbf{F} \left(2 \frac{\partial \hat{W}_{\text{std}}}{\partial \mathbf{C}} \right) + \mathbf{F} \left(2 \frac{\partial \hat{W}_{\text{AC}}}{\partial \mathbf{C}} \right) \\ &= \mathbf{F} \left(2 \frac{\partial \hat{W}_{\text{std}}}{\partial \mathbf{C}} \right) + \hat{W}_{\text{AC}} Q \mathbf{F} \left(2 \frac{\partial \hat{\alpha}_W}{\partial \mathbf{C}} \right) \end{aligned}$$

$$= \mathbf{F} \left(2 \frac{\partial \hat{W}_{\text{std}}}{\partial \mathbf{C}} \right) + 2 \hat{W}_{\text{AC}}(\mathbf{C}, Q) Q a [I_1(\bar{\mathbf{C}}) - 3] J^{-2/3} \mathbf{F} \text{Dev}^* \mathbf{G}^{-1}, \quad (48a)$$

$$\begin{aligned} \frac{\partial \hat{W}}{\partial Q} &= \frac{\partial \hat{W}_{\text{std}}}{\partial Q} + \frac{\partial \hat{W}_{\text{rem}}}{\partial Q} = \frac{\partial \hat{W}_{\text{std}}}{\partial Q} + \frac{\partial \hat{W}_{\text{AC}}}{\partial Q} \\ &= \frac{\partial \hat{W}_{\text{std}}}{\partial Q} + \mathcal{A}_0 \frac{\partial \hat{\mathcal{P}}}{\partial Q} e^{\hat{\alpha}_W Q} + \mathcal{A}_0 \hat{\mathcal{P}} e^{\hat{\alpha}_W Q} \hat{\alpha}_W, \end{aligned} \quad (48b)$$

where $\text{Dev}^* \mathbf{G}^{-1} := \mathbf{G}^{-1} - \frac{1}{3}(\mathbf{G}^{-1} : \mathbf{C}) \mathbf{C}^{-1}$ is the deviatoric part of \mathbf{G}^{-1} with respect to the deformed metric tensor \mathbf{C} . In particular, it holds that

$$\begin{aligned} \frac{\partial \hat{W}_{\text{std}}}{\partial Q} &= \frac{\Phi_{1s}}{\omega^2} \text{cov} \left(\Theta, \hat{W}_{1a}(\mathbf{C}, \hat{\mathbf{A}}(\Theta, \Phi)) \right) \\ &= \Phi_{1s} \frac{\langle \langle \Theta \hat{W}_{1a}(\mathbf{C}, \hat{\mathbf{A}}(\Theta, \Phi)) \rangle \rangle - \langle \langle \Theta \rangle \rangle \langle \langle \hat{W}_{1a}(\mathbf{C}, \hat{\mathbf{A}}(\Theta, \Phi)) \rangle \rangle}{\omega^2}, \end{aligned} \quad (49a)$$

$$\frac{\partial \hat{\mathcal{P}}}{\partial Q} = \frac{4}{(\pi/4)^4} Q \left(Q - \frac{\pi}{2} \right) \left(Q - \frac{\pi}{4} \right), \quad (49b)$$

where the notation $\mathbf{A} = \hat{\mathbf{A}}(\Theta, \Phi)$ means that the structure tensor has to be rewritten as a function of the angular coordinates Θ and Φ . The right-hand-side of (49a) is the covariance between Θ and $\hat{W}_{1a}(\mathbf{C}, \hat{\mathbf{A}}(\Theta, \Phi))$ and, since it involves the computation of directional averages, it has to be understood as a function of Q . In summary, the model equations are given by

$$\text{Div} \left[-J p \mathbf{g}^{-1} \mathbf{F}^{-T} + \mathbf{F} \left(2 \frac{\partial \hat{W}}{\partial \mathbf{C}} \right) \right] = \mathbf{0}, \quad (50a)$$

$$\dot{J} = \text{Div} (\mathbf{K} \text{Grad} p), \quad (50b)$$

$$\Gamma \dot{Q} = - \left[\frac{\partial \hat{W}}{\partial Q} - \text{Div} (D_0 \mathbf{G}^{-1} \text{Grad} Q) \right] + \mathcal{R}_{\text{ext}}, \quad (50c)$$

where the constitutive results reported in (48a)–(49b) have to be used. For the numerical computations we use the assumption that the model parameters depend only on the axial normalised coordinate $\xi = X^3/L \in [0, 1]$, with X^3 being the axial coordinate of the point $X \in \mathcal{B}$. In particular, the volumetric fractions Φ_{0s} , Φ_{1s} , and Φ_s are given by

$$\Phi_{0s} \equiv \Phi_{0s}(\xi) = -0.062 \xi^2 + 0.038 \xi + 0.046, \quad (51a)$$

$$\Phi_{1s} \equiv \Phi_{1s}(\xi) = +0.062 \xi^2 - 0.138 \xi + 0.204, \quad (51b)$$

$$\Phi_s \equiv \Phi_s(\xi) = -0.100 \xi + 0.250. \quad (51c)$$

We also introduce the void ratio $e_R(\xi) = (1 - \Phi_s(\xi))/\Phi_s(\xi)$, which is completely defined by (51c). Then, we prescribe the reference scalar permeability k_{0R} used

in (13) to be [59,38]

$$k_{0R} \equiv k_{0R}(\xi) = k_{0R}^{(0)} \left[\frac{e_R(\xi)}{e_R^{(0)}} \right]^{\kappa_0} \exp \left(\frac{1}{2} m_0 \left[\left(\frac{1 + e_R(\xi)}{1 + e_R^{(0)}} \right)^2 - 1 \right] \right), \quad (52)$$

with $k_{0R}^{(0)} = 0.003 \text{ mm}^4 \text{ N}^{-1} \text{ s}^{-1}$, $\kappa_0 = 0.0848$, $m_0 = 4.638$ [46], and $e_R^{(0)} = 4.0$ [60]. For the “standard” part of the free energy density, \hat{W}_{std} , we adopt the parameters $\alpha_0 = 0.1250 \text{ MPa}$, $\alpha_1 = 0.7778$, $\alpha_2 = 0.1111$, and $c = 7.5 \text{ MPa}$ [61] for \hat{W}_0 , \hat{W}_{1i} , and \hat{W}_{1a} (see [38] and the reference therein), and $q = 2$, $r = 1/2$, and $J_{\text{cr}}(\xi) = \Phi_s(\xi) + 0.1$ for the penalty term \hat{U} . For the remodelling part, \hat{W}_{rem} , we use several pairs of D_0 and \mathcal{A}_0 (an example of such values is $D_0 = 1.0 \cdot 10^{-4} \text{ N/rad}$ and $\mathcal{A}_0 = 154 \text{ Pa}$) and we let a take the values $a = 0$ or $a = 10^3$ (clearly, also other values may be chosen). Finally, although in a previous paper [54] we took the function

$$\omega(\xi) = 10^3 [(1 - \xi)\xi]^4 + 0.03 \quad (53)$$

to compute the variance $[\omega(\xi)]^2$, in the simulations performed for this work, we set $\omega(\xi) = \omega_0 = 0.3$ for all $\xi \in [0, 1]$.

4 The remodelling equation

In this section, we study two limit cases of the remodelling equation. The first case shows that a stationary solution of the remodelling equation recovers the profile taken from [54], which mimics the histological pattern of fibre orientation. In the second case, we search for those stationary solutions to (50c) that may represent admissible target profiles of the remodelling variable. The existence of these solutions depends on the choice of the boundary conditions.

4.1 The histological profile

As anticipated in Section 3.2, the reason for choosing the functional forms (21)–(27) is histological. To see this, let us assume that the reference, undeformed configuration of the sample coincides with the region of space that it occupies at time $t = 0$. In this configuration, the pattern of the fibre orientation can be observed experimentally, and an expression of the mean angle fitting the histological data is given by [54]

$$Q_{\text{fit}}(\xi) = \frac{\pi}{2} \left\{ 1 - \cos \left(\frac{\pi}{2} \left[-\frac{2}{3} \xi^2 + \frac{5}{3} \xi \right] \right) \right\}, \quad (54)$$

where ξ is the normalised axial coordinate. The coordinate ξ is zero at the bone-cartilage interface (also known as “tidemark”), which coincides with the sample’s lower boundary $(\partial\mathcal{B})_L$, and is equal to unity at the articular surface, represented by the upper boundary $(\partial\mathcal{B})_U$. Note that, in this configuration,

the fluid is assumed to be at rest and the pore pressure is taken equal to zero everywhere in the tissue. The function Q_{fit} takes the values $Q_{\text{fit}}(0) = 0 \text{ rad}$ and $Q_{\text{fit}}(1) = \pi/2 \text{ rad}$, thereby meaning that the fibres are almost perfectly parallel to the specimen's symmetry axis at the tidemark, and almost perfectly orthogonal to it at the articular surface. Thus, by construction, Q_{fit} mimics the histological profile of the fibre mean angle.

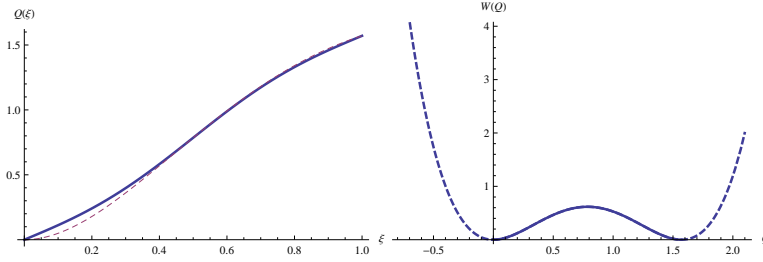


Fig. 2 (a): Comparison between $Q_{\text{fit}}(\xi)$ and $Q(\xi)$ for a given set of parameters \mathcal{A}_0 , D_0 , and specimen height L . For the chosen parameters, the two curves deviate appreciably from each other only for values of ξ close to zero, i.e., in the deep zone of articular cartilage. (b): The Allen-Cahn free energy density in (26) is represented. The dashed parts lie outside of the considered range $[0, \pi/2]$. In fact, the two minima correspond to $Q(0) = 0 \text{ rad}$ and $Q(1) = \pi/2 \text{ rad}$, respectively.

We take inspiration from the aforementioned experimental observations to claim that the angles $Q_{\text{fit}}(0) = 0 \text{ rad}$ and $Q_{\text{fit}}(1) = \pi/2 \text{ rad}$ are “critical” values of the fibre mean angle and, more importantly, that the histological profile is the result of a “structural phase transition” occurring in articular cartilage at some stage of its formation (thus, *prior* to any mechanical test performed on the tissue either *in vitro* or *in silico*). In our view, this phase transition consists of a structural reorganisation of the tissue, and leads to the histological fibre distribution observed in the undeformed configuration. To see whether our interpretation is compatible with experimental evidence, we endow the tissue with a free energy density of the Allen-Cahn type, which we assume to exist independently of deformation, and we suggest that the histological profile is the solution of a variational problem formulated in the undeformed configuration. In fact, we choose $\hat{W}_{\text{rem}}^{(0)}(Q, \text{Grad } Q)$ as specified in (24a), with $\hat{W}_{\text{str}}^{(0)}(Q) = \hat{W}_{\text{AC}}^{(0)}(Q)$ as in (26), and we require the functional derivative of $\mathcal{W}_{\text{rem}}^{(0)}$ [see Eq. (25)] to be zero. This amounts to solving the partial differential equation

$$\frac{\partial \hat{W}_{\text{rem}}^{(0)}}{\partial Q} - \text{Div} \left[\frac{\partial \hat{W}_{\text{rem}}^{(0)}}{\partial \text{Grad } Q} \right] = 0 \quad \Rightarrow \quad (55a)$$

$$\frac{\partial \hat{W}_{\text{AC}}^{(0)}}{\partial Q} - \text{Div} [D_0 \mathbf{G}^{-1} \text{Grad } Q] = 0 \quad \Rightarrow \quad (55b)$$

$$\frac{4\mathcal{A}_0}{(\pi/4)^4}Q\left(Q - \frac{\pi}{2}\right)\left(Q - \frac{\pi}{4}\right) - \text{Div}[D_0\mathbf{G}^{-1}\text{Grad}Q] = 0. \quad (55c)$$

Let us now focus on a particularly simple case in which the sample is a cylinder (as specified in section 3.4), and Q depends only on the normalised axial coordinate ξ . The coefficient D_0 is set equal to zero from the outset when the spatial resolution of the remodelling variable is not explicitly taken into account, and is greater than zero otherwise. According to these hypotheses, when $D_0 \neq 0$, (55c) becomes

$$\frac{4\mathcal{A}_0L^2}{(\pi/4)^4D_0}Q\left(Q - \frac{\pi}{2}\right)\left(Q - \frac{\pi}{4}\right) - \frac{d^2Q}{d\xi^2} = 0, \quad (56)$$

with the boundary conditions $Q(0) = 0$ rad and $Q(1) = \pi/2$ rad. Comparing the solution of (56), $Q_h(\xi)$, with the function $Q_{\text{fit}}(\xi)$ assigned in (54) allows to estimate the combination of parameters \mathcal{A}_0 and D_0 that minimises the distance between $Q_h(\xi)$ and $Q_{\text{fit}}(\xi)$ (see Fig. 2). This result seems to suggest that, after the model parameters are calibrated on the basis of experimental observations, and the histologically based boundary conditions $Q(0) = 0$ rad and $Q(1) = 0$ rad are enforced, the functional form of the histological profile need not be prescribed by fitting experimental data, since it may be computed as the extremum of the remodelling energy (25).

As anticipated in Section 3.4, the Dirichlet boundary conditions imposed on the values taken by Q at the lower and upper boundary of the sample enhance the convergence of the solution towards Q_{fit} . This behaviour, however, manifests itself only at $(\partial\mathcal{B})_L$ and $(\partial\mathcal{B})_U$, where the conditions (45a) and (45b) comply with the minimum configurations of $\hat{W}_{AC}^{(0)}(Q)$. In general, instead, when the evolution of the fibre mean angle is studied in conjunction with the deformation of the tissue, our model can produce a profile that is far from the histological one (see e.g. Fig. (8)). Moreover, other boundary conditions, which may depend on time, deformation, or stress, could also be considered to better describe other physical occurrences.

We remark that the profile reported in Fig. 2(a) has been obtained for $L = 1$ mm and the ratio $(\mathcal{A}_0L^2)/D_0 = 1.54$. A pair of model parameters \mathcal{A}_0 and D_0 complying with this ratio is given by $D_0 = 1.0 \cdot 10^{-4}$ N/rad and $\mathcal{A}_0 = 154$ Pa.

4.2 “Target fields” and stationary solutions

An essential issue in the mechanical theories of remodelling is the identification of the generalised forces that drive the structural evolution of the considered system. Before studying this problem within our theoretical framework, we review the case in which the free energy density does not feature terms of the type $\hat{W}_{\text{rem}}(\mathbf{C}, Q, \text{Grad}Q)$. In such a setting, the remodelling law (50c) reduces to the ordinary differential equation

$$\Gamma\dot{Q} = \mathcal{R}_{\text{ext}} - \frac{\partial\hat{W}_{\text{std}}}{\partial Q}(\mathbf{C}, Q), \quad (57)$$

and the evolution of Q is entirely driven by the difference between \mathcal{R}_{ext} and $\partial\hat{W}_{\text{std}}/\partial Q$. More specifically, while $\partial\hat{W}_{\text{std}}/\partial Q$ is dictated by the choice of \hat{W}_{std} , \mathcal{R}_{ext} characterises the coupling between Q and the other mechanical variables of the system. For example, following Hariton et al. [62], \mathcal{R}_{ext} may be related to stress by claiming that the direction along which the fibres tend to align themselves is driven by the eigenvalues of Cauchy stress tensor. To account for this requirement, it is possible to prescribe \mathcal{R}_{ext} as [27]

$$\mathcal{R}_{\text{ext}} \equiv \frac{\partial\hat{W}_{\text{std}}}{\partial Q}(\mathbf{C}, Q_{\text{T}}), \quad (58)$$

where Q_{T} is a suitably constructed *target angle*, i.e., a “privileged” distribution of the mean angle entirely determined by stress. We emphasise that, since the principal stresses are time-dependent, the target angle varies in time [27]. Thus, \dot{Q} is generally non-zero until Q is not equal to Q_{T} . If, however, (57) and (58) are studied in the limit in which Q_{T} tends to some stationary distribution Q_{T}^{∞} , the remodelling process ceases asymptotically when Q approaches one of the stationary solutions of the evolution equation

$$\Gamma\dot{Q} = \frac{\partial\hat{W}_{\text{std}}}{\partial Q}(\mathbf{C}, Q_{\text{T}}^{\infty}) - \frac{\partial\hat{W}_{\text{std}}}{\partial Q}(\mathbf{C}, Q). \quad (59)$$

In particular, if the dependence of \hat{W}_{std} on Q implies the uniqueness of the stationary solution to (59), then $Q_{\text{st}} \equiv Q_{\text{T}}^{\infty}$ is the stationary mean angle towards which the system remodels.

We remark that the existence of solutions of the type $Q_{\text{st}} = Q_{\text{T}}^{\infty}$ is closely related to the introduction of the target angle and the external remodelling force, \mathcal{R}_{ext} . In a previous work [39], however, we searched for stationary solutions to (57) in the limit case of vanishing, or negligibly small, \mathcal{R}_{ext} and with \hat{W}_{std} defined as in (18)–(20c). Consequently, we solved the remodelling equation

$$\Gamma\dot{Q} = -\frac{\partial\hat{W}_{\text{std}}}{\partial Q}, \quad (60)$$

and we found that \dot{Q} tended asymptotically towards zero because the condition

$$0 = -\frac{\partial\hat{W}_{\text{std}}}{\partial Q} = -\frac{\Phi_{1s}}{\omega^2} \text{cov}\left(\Theta, \hat{W}_{1a}(\mathbf{C}, \hat{\mathbf{A}}(\Theta, \Phi))\right) \quad (61)$$

applied for large values of t . This result was respected because the deformation obtained for large values of t implied the asymptotic fulfilment of the inequality $I_4 \leq 1$, even though (61) admitted no roots in the variable Q . We remark *a posteriori* that, if \mathcal{R}_{ext} had been considered in [39] in the form given in (58), the presence of the Heaviside function $\mathcal{H}(I_4 - 1)$ in the definition of \hat{W}_{std} would have made it tend asymptotically towards zero for the deformations attained in the tissue for large times.

The theoretical setting developed in this work is conceived to improve the results obtained in [39]. To this end, it proposes to describe remodelling through (50c), which introduces two novelties: It accounts for the spatial resolution of the fibre mean angle, and it defines the remodelling part of the system's free energy density, \hat{W}_{rem} , where $\exp(\hat{\alpha}_W(\mathbf{C})Q)$ describes a non-trivial coupling between Q and the deformation [see (31b) and (28)]. By enforcing the simplifying assumptions done in Section 3.4, and neglecting \mathcal{R}_{ext} from the outset, the remodelling equation (50c) becomes

$$\Gamma \dot{Q} = \text{Div} [D_0 \mathbf{G}^{-1} \text{Grad} Q] - \frac{\partial \hat{W}_{\text{AC}}}{\partial Q} - \frac{\partial \hat{W}_{\text{std}}}{\partial Q}. \quad (62)$$

Note that, similarly to \mathcal{R}_{ext} in (57), also the term $-\partial \hat{W}_{\text{AC}}/\partial Q$ plays a “driving” role in the evolution of the fibre mean angle and, in fact, we switch off \mathcal{R}_{ext} with the purpose of focussing on the implications of $-\partial \hat{W}_{\text{AC}}/\partial Q$ on remodelling. In this case, since no stress-driven target angle is considered *a priori* in the model, $-\partial \hat{W}_{\text{AC}}/\partial Q$ modulates the evolution of Q through the deformation. In this framework, however, a “target angle” is—if it exists—a stationary solution to (62), i.e., a function obtained by solving

$$-\left[\frac{\partial \hat{W}_{\text{std}}}{\partial Q} + \frac{\partial \hat{W}_{\text{AC}}}{\partial Q} - \text{Div} (D_0 \mathbf{G}^{-1} \text{Grad} Q) \right] = 0, \quad (63)$$

together with (50a), (50b), and the boundary conditions prescribed in Section 3.4. For example, in the case of articular cartilage, we impose $Q(X) = 0$ rad for $X \in (\partial \mathcal{B})_{\text{L}}$ and $Q(X) = \pi/2$ rad for $X \in (\partial \mathcal{B})_{\text{U}}$, thereby requiring the congruence of Q with the initial histological data for all the points of the lower boundary, $(\partial \mathcal{B})_{\text{L}}$, and for all the points of the upper boundary, $(\partial \mathcal{B})_{\text{U}}$, of the cartilage specimen taken for benchmarking (note that the dependence of Q on time has been suppressed here, because we are looking for stationary solutions). We notice that, notwithstanding their similar form, (63) is quite different from (55c). The differences are essentially due to two facts. Firstly, in (63), both the contribution to remodelling stemming from the standard strain energy density, \hat{W}_{std} , and the Allen-Cahn contribution, \hat{W}_{AC} , are accounted for. Secondly, in (63), \hat{W}_{AC} takes into account the coupling between deformation and remodelling, since it depends both on \mathbf{C} and on Q . In particular, the introduction of the factor $\exp(\hat{\alpha}_W(\mathbf{C})Q)$ shifts, for a given \mathbf{C} , the maximum configuration of $\hat{W}_{\text{AC}}(\mathbf{C}, Q)$ from $\pi/4$ to the deformation dependent value

$$Q_{\text{max}} \equiv Q_{\text{max}}(\mathbf{C}) = \frac{-8 + \pi \hat{\alpha}_W(\mathbf{C}) + \sqrt{64 + \pi^2 [\hat{\alpha}_W(\mathbf{C})]^2}}{4 \hat{\alpha}_W(\mathbf{C})}, \quad (64)$$

for $\hat{\alpha}_W(\mathbf{C}) \neq 0$. In the limit of vanishing $\hat{\alpha}_W(\mathbf{C})$, the value $Q_{\text{max}} = \pi/4$ rad is recovered.

In the following, we speak of “*standard remodelling*” when we refer to (60), and we call “*non-standard remodelling*” the process described by (62).

5 Numerical Tests

In this section, we report the results of the Finite Element implementation of the unconfined compression test described in Section 3.4. To this end, we consider the weak form of the model equations (50a)–(50c) associated with the BCs (43a)–(43c) and (45a)–(45c), i.e.,

$$\mathcal{F}(\chi, p, Q) = \mathcal{F}_\chi(\chi, p, Q) + \mathcal{F}_p(\chi, p, Q) + \mathcal{F}_Q(\chi, Q) = 0, \quad (65)$$

where the functionals \mathcal{F}_χ , \mathcal{F}_p , and \mathcal{F}_Q are defined as

$$\mathcal{F}_\chi(\chi, p, Q) = \int_{\mathcal{B}} \left[-Jp \mathbf{g}^{-1} \mathbf{F}^{-T} + \hat{\mathbf{P}}_{\text{sc}}(\mathbf{F}, Q) \right] : \mathbf{g} \text{Grad } \tilde{\mathbf{u}}, \quad (66a)$$

$$\mathcal{F}_p(\chi, p, Q) = \int_{\mathcal{B}} \left[J\tilde{p} + (\text{Grad } \tilde{p}) \hat{\mathbf{K}}(\mathbf{C}, Q)(\text{Grad } p) \right], \quad (66b)$$

$$\begin{aligned} \mathcal{F}_Q(\chi, Q) &= \int_{\mathcal{B}} [D_0 \mathbf{G}^{-1} \text{Grad } Q] \text{Grad } \tilde{\Omega} \\ &+ \int_{\mathcal{B}} \left[\Gamma \dot{Q} + \frac{\partial \hat{W}_{\text{std}}}{\partial Q}(\mathbf{C}, Q) + \frac{\partial \hat{W}_{\text{AC}}}{\partial Q}(\mathbf{C}, Q) \right] \tilde{\Omega}. \end{aligned} \quad (66c)$$

Here, $\tilde{\mathbf{u}}$ and $\tilde{\Omega}$ are the test velocities associated with the solid phase motion, χ , and the mean angle, Q , respectively, and \tilde{p} is the test pressure.

Equations (66a)–(66c) are discretised in time and, at each time step, they are solved with the aid of a linearisation method. This requires to compute the directional averages that define $\hat{\mathbf{P}}_{\text{sc}}$, $\hat{\mathbf{K}}$, and $\partial \hat{W}_{\text{std}}/\partial Q$, along with their derivatives (such derivatives, indeed, appear in the linearisation scheme). In fact, the evaluation of these averages is accomplished by having recourse to the numerical procedure known as Spherical Design Algorithm (SDA) [63]. Since presenting the whole procedure is rather lengthy and out of the scope of our work, we show here only the construction of $\partial \hat{W}_{\text{std}}/\partial Q$ (see algorithm A1).

5.1 Remodelling in the absence of deformation

In this section, we solve (62) independently of deformation. Such a situation occurs when no load is applied to the tissue (i.e., $\mathbf{g}(t)$ is zero for all times), the pore pressure is null at all times and at all points of the tissue, and no external force (such as the gravitational force) is considered. Hence, the sample is assumed to lean on the support beneath and its lower surface can be assumed to be free of surface forces. In this case, the balance laws (50a) and (50b) are trivially satisfied, and the term $\partial \hat{W}_{\text{std}}/\partial Q$ vanishes identically, so that the remodelling equation (62) becomes

$$\Gamma \dot{Q} = \text{Div} [D_0 \mathbf{G}^{-1} \text{Grad } Q] - \frac{\partial \hat{W}_{\text{AC}}}{\partial Q}, \quad (67)$$

with

$$\frac{\partial \hat{W}_{AC}}{\partial Q}(\mathbf{G}, Q) = \mathcal{A}_0 \frac{\partial \hat{\mathcal{P}}}{\partial Q}(Q) = \frac{4\mathcal{A}_0}{(\pi/4)^4} Q \left(Q - \frac{\pi}{2} \right) \left(Q - \frac{\pi}{4} \right). \quad (68)$$

We solve now (67) with the BCs (45a)–(45c) and under the hypothesis that, at the initial time of observation, the fibre mean angle $Q(X, 0)$ is a random function of X . Hence, the tissue finds itself in a disordered configuration at the initial time. We make this assumption in order to show that the Allen-Cahn model, along with the BCs (45a)–(45c), is capable of describing a change of the tissue’s material symmetry, which converts from the disordered configuration towards the ordered configuration that renders it transversely isotropic.

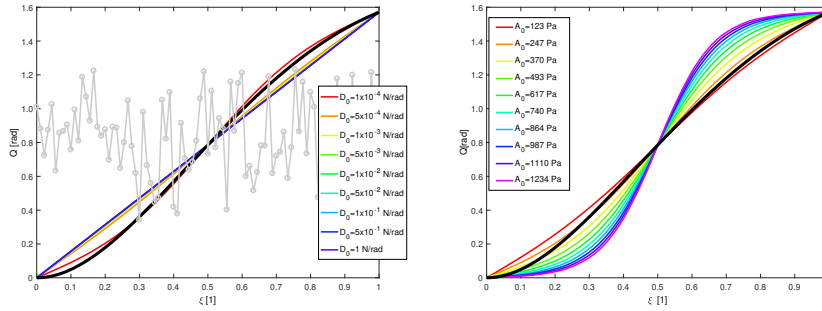


Fig. 3 Stationary profiles of the remodelling variable for different values of D_0 , with $\mathcal{A}_0 = 247$ Pa (a), and for different values of \mathcal{A}_0 , with $D_0 = 1.0 \cdot 10^{-4}$ N/rad (b). The grey circled curve in the plot on the left represents the initial profile of Q , which is set to be random.

The results of the initial-boundary value problem specified by (67), (68), and (45a)–(45c) are shown in Fig. 3 for varying values of the parameters D_0 (cf. Fig. 3a) and \mathcal{A}_0 (cf. Fig. 3b). Starting from a random profile (grey circled curve in Fig. 3a), which might represent the orientation of the fibres in an engineered tissue [64], $Q(X, t)$ evolves towards a stationary solution that is remnant of the histological profile reported in Fig. 2a. This behaviour is a consequence of the introduction of the Allen-Cahn energy density, \hat{W}_{AC} , whose two minimum configurations coincide with the boundary values imposed on Q , and manifests itself through the tendency of the remodelling variable to acquire a stationary solution interpolating between the imposed Dirichlet boundary conditions at the top (cf. (45a)) and at the bottom (cf. (45b)) of the sample. We remark that the free energy \hat{W}_{AC} generates a profile that is comparable with the histological one. In this respect we say that, in principle, the remodelling may occur also in the absence of deformation, and may be understood as a structural phase transition. Indeed, the system passes from a “phase” in which it appears to be disordered to a “phase” in which it is ordered in such a way that it is transversely isotropic. This loss, or *breaking*, of the system’s symmetries is due to the introduction of \hat{W}_{rem} .

5.2 Asymptotic “standard remodelling”

We launch a first set of simulations in which $\mathcal{R}_{\text{ext}} = 0$ and the free energy density is equal to the standard one only, i.e., $\hat{W} = \hat{W}_{\text{std}}$. In this case, the remodelling equation is given by (60) rather than (50c) and, as anticipated in Section (4.2), \hat{Q} tends towards zero for large values of t because (61) is respected asymptotically. To see why this occurs, it is necessary to determine I_4 and construct the derivative $\partial \hat{W}_{\text{std}} / \partial Q$. The latter, in turn, requires to evaluate the directional averages reported in (49a) and, thus, to use the Spherical Design Algorithm [63]. Indeed, for a given \mathbf{C} , $\partial \hat{W}_{\text{std}} / \partial Q$, is approximated as

$$\begin{aligned} \frac{\partial \hat{W}_{\text{std}}}{\partial Q}(\mathbf{C}, Q) &= \frac{\Phi_{1s}}{\omega^2} \text{cov} \left(\Theta, \hat{W}_{1a}(\mathbf{C}, \hat{\mathbf{A}}(\Theta, \Phi)) \right) \\ &= \frac{\Phi_{1s}}{\omega^2} \langle (\Theta - \langle \Theta \rangle) \hat{W}_{1a}(\mathbf{C}, \hat{\mathbf{A}}(\Theta, \Phi)) \rangle \\ &= \frac{\Phi_{1s}}{\omega^2} \int_0^{2\pi} \int_0^{\pi/2} (\Theta - \langle \Theta \rangle) \hat{W}_{1a}(\mathbf{C}, \hat{\mathbf{A}}(\Theta, \Phi)) \hat{\rho}(\Theta) \sin(\Theta) d\Theta d\Phi \\ &\approx \frac{\Phi_{1s}}{\omega^2} \frac{2\pi}{N} \sum_{i=1}^m \sum_{j=1}^n (\Theta_i - \langle \Theta \rangle) \hat{W}_{1a}(\mathbf{C}, \mathbf{A}_{ij}) \hat{\rho}(\Theta_i), \end{aligned} \quad (69)$$

where $N = mn$ is the total number of quadrature points used for the numerical solution of the integral in (69), $\mathcal{I} \times \mathcal{J} \subset [0, \pi/2] \times [0, \pi]$ is the set of all quadrature points, and, for each $(\Theta_i, \Phi_j) \in \mathcal{I} \times \mathcal{J}$, we write $\mathbf{A}_{ij} = \mathbf{M}_{ij} \otimes \mathbf{M}_{ij}$ (no sum with respect to i and j), with $\mathbf{M}_{ij} = \hat{\mathbf{M}}(\Theta_i, \Phi_j)$. Hence, $\hat{W}_{1a}(\mathbf{C}, \mathbf{A}_{ij})$ is rewritten as

$$\hat{W}_{1a}(\mathbf{C}, \mathbf{A}_{ij}) = \mathcal{H}(I_4(\mathbf{C}, \mathbf{A}_{ij}) - 1)^{\frac{1}{2}c} [I_4(\mathbf{C}, \mathbf{A}_{ij}) - 1]^2. \quad (70)$$

Note that \mathcal{I} and \mathcal{J} are sets of points suitably chosen in $[0, \pi/2]$ and $[0, 2\pi]$, respectively [40].

As prescribed in lines 21 and 22 of the pseudo-code of Algorithm A1, the summand of (69) with indices i and j contributes to $\partial \hat{W}_{\text{std}} / \partial Q$ only if $\hat{\rho}(\Theta_i)$ is greater than a given threshold value, tol_Ψ , and $I_4(\mathbf{C}, \mathbf{A}_{ij}) > 1$. The first control is, in fact, on the probability density that a fibre is aligned along the direction specified by $(\Theta_i, \Phi_j) \in \mathcal{I} \times \mathcal{J}$. The second condition, instead, represents the algorithmic formulation of the Heaviside function in (70).

To have indications about these restrictions, we study the time evolution of $I_4(\mathbf{C}, \mathbf{A}_{ij})$ and $\hat{\rho}$ at two selected points of the sample, for different values of Θ . The results are reported in Fig. 4, where the black curves represent constant values for I_4 and $\hat{\rho}$, taken as reference (here, we choose $I_4^{(0)} = 1$ and $\hat{\rho}^{(0)} = \text{tol}_\Psi$). Moreover, the point of coordinates $X_L = (0, 0, L/4)$ finds itself in the deep zone of the sample, in which the fibres tend to be parallel to the symmetry axis of the cylinder and, thus, perpendicular to the lower boundary (this corresponds to the bone-cartilage interface when the tissue is *in vivo*). The point of coordinates $X_U = (0, 0, 3L/4)$, instead, is situated in

Algorithm 1 –A5– Spherical Design Algorithm (SDA) for the evaluation of (49a) and (69) within the p th time step and the ℓ th linearisation iteration

```

1: procedure SDA
2:   for  $k = 1, \dots, M$  do ( $M$  is the number of grid nodes)
3:     Initialise  $\left(\frac{\partial \hat{W}_{\text{std}}}{\partial Q}\right)^{p\ell k} = 0$ , and  $\mathcal{Z}^{p\ell k} = 2\pi \int_0^{\pi/2} \hat{\gamma}^{p\ell k}(\Theta) \sin \Theta d\Theta = 0$  (partial sums)
4:     Load the point set  $\{(\Theta_i, \Phi_j)\}_{i,j=1}^{N=mn} \subset \mathcal{I} \times \mathcal{J}$ 
5:     Load  $Q^{p\ell k} = Q^\ell(X_k, t_p)$  and  $\omega^k = \omega(\xi_k)$ 
6:     for  $i = 1, \dots, m$  do (inner cycle to evaluate the normalisation factor)
7:       Evaluate  $\hat{\gamma}^{p\ell k}(\Theta_i) = \exp\left(-\frac{(\Theta_i - Q^{p\ell k})^2}{2[\omega^k]^2}\right)$ 
8:        $\mathcal{Z}^{p\ell k} = \mathcal{Z}^{p\ell k} + \frac{2\pi}{N} \hat{\gamma}^{p\ell k}(\Theta_i)$ 
9:     end for
10:    Calculate  $\hat{\phi}^{p\ell k}(\Theta_i) = \frac{\hat{\gamma}^{p\ell k}(\Theta_i)}{\mathcal{Z}^{p\ell k}}$ ,  $i = 1, \dots, m$ 
11:    for  $i = 1, \dots, m$  do inner cycle to determine  $\langle \Theta \rangle^{p\ell k}$ 
12:      if  $\hat{\phi}^{p\ell k}(\Theta_i) > \text{tol}_\Psi$  then
13:         $\langle \Theta \rangle^{p\ell k} = \langle \Theta \rangle^{p\ell k} + \frac{2\pi}{N} \Theta_i \hat{\phi}^{p\ell k}(\Theta_i)$ 
14:      end if
15:    end for
16:    Given  $\mathbf{C}^{p\ell k}$ :
17:    for  $i = 1, \dots, m$  do
18:      for  $j = 1, \dots, n$  do
19:        Evaluate  $I_4(\mathbf{C}^{p\ell k}, \mathbf{A}_{ij}) = \mathbf{C}^{p\ell k} : \mathbf{A}_{ij}$ , and
20:         $\mathbf{A}_{ij} = \mathbf{M}_{ij} \otimes \mathbf{M}_{ij}$ , with  $\mathbf{M}_{ij} = \hat{\mathbf{M}}(\Theta_i, \Phi_j)$ 
21:        if  $\hat{\phi}^{p\ell k}(\Theta_i) > \text{tol}_\Psi$  then
22:          if  $I_4(\mathbf{C}^{p\ell k}, \mathbf{A}_{ij}) > 1$  then
23:            Evaluate
24:             $\mathcal{R}^{p\ell k}(\Theta_i, \Phi_j) = \frac{\Phi_{1s}(X_k)}{[\omega^k]^2} (\Theta_i - \langle \Theta \rangle)^{\frac{1}{2}c} \left[ I_4(\mathbf{C}^{p\ell k}, \mathbf{A}_{ij}) - 1 \right]^2 \hat{\phi}^{p\ell k}(\Theta_i)$ 
25:             $\left(\frac{\partial \hat{W}_{\text{std}}}{\partial Q}\right)^{p\ell k} = \left(\frac{\partial \hat{W}_{\text{std}}}{\partial Q}\right)^{p\ell k} + \frac{2\pi}{N} \mathcal{R}^{p\ell k}(\Theta_i, \Phi_j)$ 
26:          end if
27:        end if
28:      end for
29:    end for
30:  end for
31: end procedure

```

the superficial zone, in which the fibres are parallel to the upper boundary (which corresponds to the articular surface of the tissue *in vivo*).

Looking at the left column of Fig. 4, obtained for $X_U = (0, 0, 3L/4)$, we see that the curves corresponding to $I_4(\mathbf{C}, \hat{\mathbf{A}}(2\pi/5, \Phi))$ and $I_4(\mathbf{C}, \hat{\mathbf{A}}(\pi/2, \Phi))$ are above 1 for all the duration of the experiment, and tend to unity from above for large times. Thus, at least in principle, the fibres aligned along $\hat{\mathbf{M}}(2\pi/5, \Phi)$ and $\hat{\mathbf{M}}(\pi/2, \Phi)$ contribute to $\partial \hat{W}_{\text{std}} / \partial Q$. However, the corresponding probability densities become smaller than tol_Ψ as times goes by, thereby ruling out the fibres oriented parallel to $\hat{\mathbf{M}}(2\pi/5, \Phi)$ and $\hat{\mathbf{M}}(\pi/2, \Phi)$. The curve corresponding to $I_4(\mathbf{C}, \hat{\mathbf{A}}(\pi/3, \Phi))$ is above 1 up to a certain instant of time subsequent T_{ramp} , and goes below 1 afterwards. Thus, the fibres aligned along $\hat{\mathbf{M}}(\pi/3, \Phi)$ do not contribute to $\partial \hat{W}_{\text{std}} / \partial Q$. Finally, all other curves are below 1 for all the duration of the experiment and give, then, no contribution to (69).

The right column of Fig. 4, which refers to $X_L = (0, 0, L/4)$, shows that the curve $I_4(\mathbf{C}, \hat{\mathbf{A}}(\pi/2, \Phi))$ is the only one that remains above 1, even though it tends to unity for large values of t . The corresponding probability density,

however, goes below tol_Ψ after T_{ramp} , thereby nullifying the contribution to (69) stemming from the fibres oriented along $\hat{\mathbf{M}}(\pi/2, \Phi)$. In conclusion, Fig. 4 indicates that, for sufficiently large values of t , $\partial \hat{W}_{\text{std}} / \partial Q$ tends towards zero because the deformation established in the sample and the values taken by the probability density switch off all the contributions of the sum (69).

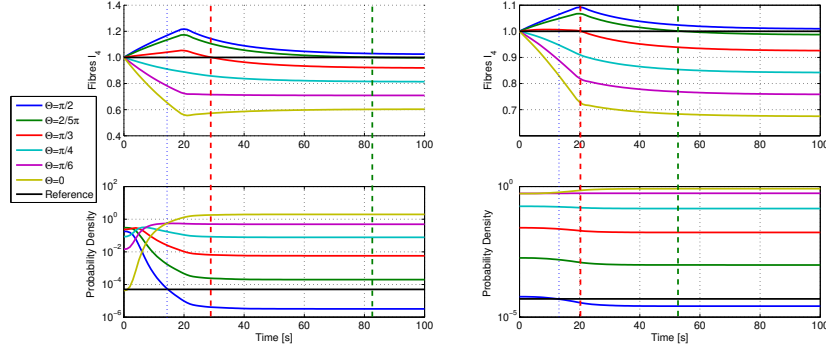


Fig. 4 Time evolution of $I_4(C, \hat{\mathbf{A}}(\Theta, \Phi))$ and $\bar{\varphi}_X(\Theta)$ at $\Theta \in \mathcal{J} = \{0, \frac{\pi}{6}, \frac{\pi}{4}, \frac{\pi}{3}, \frac{2\pi}{5}, \frac{\pi}{2}\}$. Note that, for the computed deformation, $I_4(C, \hat{\mathbf{A}}(\Theta, \Phi))$ is independent of Φ . The figures in the left column correspond to the point of coordinates $X_U = (0, 0, 3L/4)$; those in the right column to the point of coordinates $X_L = (0, 0, L/4)$.

5.3 “Standard” versus “non-standard” remodelling

It is worth to remark that, as long as it holds that $\hat{W} = \hat{W}_{\text{std}}$, the parameter Γ determines the stationary value of Q for a given loading time. Once this value is reached, if no additional compression is applied to the sample, then $\dot{Q} = 0$ applies and no further evolution is observed. On the contrary, when the free energy density is given by $\hat{W} = \hat{W}_{\text{std}} + \hat{W}_{\text{rem}}$, with \hat{W}_{rem} specified in (31b), remodelling continues even when $\partial \hat{W}_{\text{std}} / \partial Q$ becomes negligibly small. This further evolution of the mean angle is induced by \hat{W}_{rem} only. The described behaviour is represented in Figs. 5 and 6, where the evolution of Q and $-\Gamma \dot{Q}$ over time is shown both in the case of “standard” and in the case of “non-standard” remodelling. Note that Figs. 5 and 6 are obtained by evaluating Q in $X_L = (0, 0, L/4)$ and $X_U = (0, 0, 3L/4)$, respectively.

“Standard” remodelling predicts that both $Q(X_L, t)$ and $Q(X_U, t)$ decrease monotonically towards asymptotically constant values (see Figs. 5a and 6a). This behaviour is consistent with the trend of $-\Gamma \dot{Q}$ shown in Figs. 5b and 6b. Indeed, since $-\Gamma \dot{Q}(X_L, t)$ and $-\Gamma \dot{Q}(X_U, t)$ are both non-negative for all times, and Γ is strictly positive, the derivatives $\dot{Q}(X_L, t)$ and $\dot{Q}(X_U, t)$ are non-positive for all times. “Non-standard” remodelling, instead, destroys the

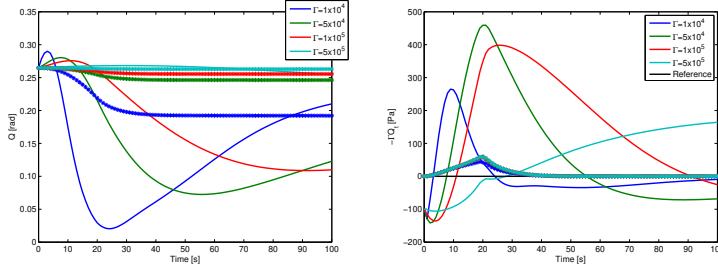


Fig. 5 (a): Time evolution of the mean angle Q . (b) Time evolution of $-\Gamma \dot{Q}$ (note that, in the label, the notation $Q_t \equiv \dot{Q}$ has been used). The dashed curves with asterisks refer to “standard” remodeling. The solid curves refer to “non-standard” remodeling for $a = 0$. All curves are obtained by evaluating both Q and $-\Gamma \dot{Q}$ in $X_L = (0, 0, L/4)$. The units of Γ are J s m^{-3} .

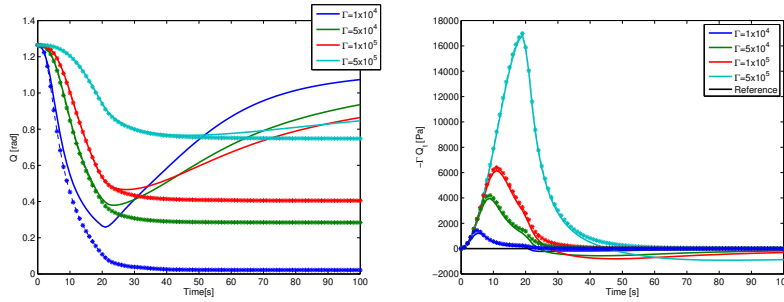


Fig. 6 (a): Time evolution of the mean angle Q . (b) Time evolution of $-\Gamma \dot{Q}$ (note that, in the label, the notation $Q_t \equiv \dot{Q}$ has been used). The dashed curves with asterisks refer to “standard” remodeling. The solid curves refer to “non-standard” remodeling for $a = 0$. All curves are obtained by evaluating both Q and $-\Gamma \dot{Q}$ in $X_U = (0, 0, 3L/4)$. The units of Γ are J s m^{-3} .

monotonicity of the curves $Q(X_L, t)$ and $Q(X_U, t)$, and slows down the rate by which they approach a stationary value.

From Fig. 5 we see that, in the case of “standard” remodeling, the variation of both $Q(X_L, t)$ and $-\Gamma \dot{Q}(X_L, t)$ is markedly smaller than it is in the case of “non-standard” remodeling. This behaviour is mainly due to the fact that the initial preferential direction of the fibres is close to the one that is parallel to the symmetry axis of the sample. Thus, for almost all fibres it holds $I_4 \leq 1$. In other words, the term $-\Gamma \dot{Q}$ in (60) (“standard” case) is much smaller than $-\Gamma \dot{Q}$ in (62) (“non-standard” case). In addition, we remark that, when the free energy density \hat{W}_{rem} is introduced, the quantity $-\Gamma \dot{Q}(X_L, t)$ is different from zero at $t = 0$ s. This is due to the fact that, at $t = 0$ s, \hat{W}_{std} is equal to the unessential constant α_0 , while \hat{W}_{rem} is non-trivial, because the gradient of Q is not null at $X = X_L$, and the value $Q(X_L, 0) \approx 0.265$ rad is sufficiently far away from the zeroes of $\partial \hat{W}_{\text{AC}} / \partial Q$ (at $t = 0$ s, they are $Q = 0$ rad, $Q = \pi/4$ rad, and $Q = \pi/2$ rad). For $t \geq 0$, $-\Gamma \dot{Q}(X_L, t)$ grows during the first instants of time of the loading ramp, thereby leading to a decrease of Q ,

and reaches an absolute maximum. Then, it goes below zero and tends again towards an asymptotic value. This trend, however, seems not to be followed for $\Gamma = 5.0 \cdot 10^5 \text{ J s m}^{-3}$ (see Fig. 5b), even though both $Q(X_L, t)$ and $-\Gamma Q(X_L, t)$ converge to stationary values for sufficiently long times.

In contrast to what is observed in Fig. 5, we see in Fig. 6 that \hat{W}_{rem} does not affect appreciably the trend of the remodelling variable in the course of the loading ramp, i.e., for $t \in [0, T_{\text{ramp}}]$. For $t \geq T_{\text{ramp}}$, instead, the “standard” remodelling predicts a final value of Q that is constant in time and lower than the initial one, whereas \hat{W}_{rem} drives the growth of Q up to an asymptotic value that comes nearer to the initial one, with a rate of convergence ruled by Γ . We remark that, in “standard” remodelling, the parameter Γ is the only quantity that controls the stationary value of Q .

Finally, the strongest differences between the two compared models are at the final time of observation and in the relaxation times. Indeed, in the case of “non-standard” remodelling, the energetic contribution \hat{W}_{rem} is predominant in ruling the behaviour of the remodelling variable after the loading ramp, thus when $\partial \hat{W}_{\text{std}} / \partial Q$ tends towards zero, thereby mainly affecting the final state of the system.

In Fig. 7a, we report the axial profile of the circumferential component of the second Piola-Kirchhoff stress tensor *due to the fibres*, i.e.

$$\mathbf{S}_a = 2\Phi_{1s}(\partial \langle \hat{W}_{1a} \rangle / \partial \mathbf{C}),$$

evaluated at $T_{\text{end}} = 100 \text{ s}$. As expected, the occurrence of remodelling lowers the stress in the tissue in comparison with the case of no remodelling. We remark, however, that in the case of “non-standard” remodelling the stress behaviour is related to the choice of the boundary conditions imposed on Q . Indeed, the fact that in this work Q is constrained to be equal to $\pi/2 \text{ rad}$ at the upper boundary of the sample (see also Fig. 7b) produces in that zone a value of stress equal to the one obtained in the absence of remodelling. The “standard” remodelling, instead, for which no boundary conditions on Q are required, reduces the stress everywhere in the sample. The deviation is evident in the superficial (upper) zone of the sample, where the mean angle evolves the most (cf. Fig. 7b), and is barely visible in the deep (lower) zone, in which almost no remodelling occurs (see also the trend of Q shown in Fig. 7b).

In Fig. 8, we report the axial profile of the mean angle for $t \geq T_{\text{ramp}}$. In particular, by expressing Q as a function of the normalised axial coordinate and time, and recalling the parameter a introduced in (46), we compare the shape of $Q(\xi, t)$ computed for $a = 0$ with that obtained for $a \neq 0$. For $a = 0$ (Fig. 8a), the plot of the mean angle tends to recover its initial shape for $t > T_{\text{ramp}}$. For $a \neq 0$ (Fig. 8b), instead, the curves obtained for $t > T_{\text{ramp}}$ evolve in time while maintaining a shape similar to the curve determined for $t = T_{\text{ramp}}$. Since the profile of the mean angle is a representation of the pattern of fibre orientation in the sample, we conclude that, as expected, the introduction of a non-vanishing parameter a brings about structural changes that are more pronounced than in the case $a = 0$. This may be due to the fact that the condition $a \neq 0$ activates the term $\mathcal{A}_0 e^{\hat{\alpha}_W(\mathbf{C})Q} \hat{\alpha}_W(\mathbf{C}) \hat{\mathcal{P}}(Q)$ on the

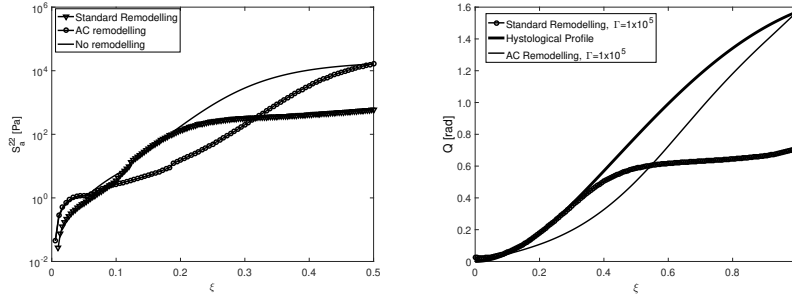


Fig. 7 (a) Circumferential component of the anisotropic part of the second Piola-Kirchhoff stress tensor, $(S_a)^{22}$ evaluated along the symmetry axis for $t = T_{\text{end}}$. (b) Axial profile of the mean angle for $t = T_{\text{end}}$. Note that the curves labelled with “AC remodelling” refer to the “non-standard” remodelling and are obtained with $a = 0$. The units of Γ are J s m^{-3} .

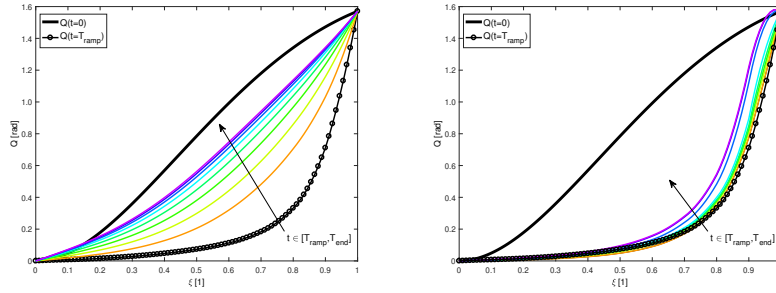


Fig. 8 Axial profile of Q for $t \geq T_{\text{ramp}}$ in the case $a = 0$ (a) and $a = 10^3$ (b). For both cases, we set $\Gamma = 1.0 \cdot 10^4 \text{ J s m}^{-3}$.

right-hand-side of (48b), which gives rise to an additional remodelling force. This, in turn, may be responsible for the marked change of the mean angle also in the deep zone of the tissue (i.e., for values of ξ closer to zero), where otherwise only small changes of the mean angle are observed for $a = 0$. Indeed, when a is set equal to zero, the right-hand-side of (48b) reduces to

$$\frac{\partial \hat{W}}{\partial Q} = \frac{\partial \hat{W}_{\text{std}}}{\partial Q} + \mathcal{A}_0 \frac{\partial \hat{P}}{\partial Q}, \quad (71)$$

and, since $\partial \hat{W}_{\text{std}} / \partial Q$ goes to zero for large times, the remodelling force $\partial \hat{W} / \partial Q$ that remains active also in the limit of large t , i.e., $\mathcal{A}_0 \partial \hat{P} / \partial Q$, is independent of deformation. This means that, for $a = 0$, the remodelling becomes asymptotically decoupled from deformation.

6 Summary of results and further research

The remodelling considered in our work consists of the reorientation of the collagen fibres of a fibre-reinforced, hydrated soft tissue (e.g. articular cartilage),

in which the fibres are aligned according to a prescribed probability density. The remodelling process is described through the spatiotemporal evolution of the mean angle associated with the fibre probability density. The mean angle is determined by solving the balance of generalised forces presented in (10), in which the generalised forces \mathcal{R}_{ext} and \mathcal{R}_{int} are said to be external and internal remodelling forces, respectively. The force \mathcal{R}_{int} is assigned constitutively. To this end, and motivated by histological observations, we proposed a constitutive theory based on the introduction of the remodelling free energy density \hat{W}_{rem} . This takes the spatial resolution of the mean angle explicitly into account, and features the Allen-Cahn term \hat{W}_{AC} , whose minimum configurations coincide with the mean angles at the lower and upper boundary of the sample.

Our first result is that our model determines the histological profile of the mean angle as the solution of a partial differential equation, rather than by fitting experimental data (see Fig. 2). This result, however, follows also from the choice of the boundary conditions, and a histologically based calibration of the model parameters D_0 and \mathcal{A}_0 . We interpreted this result as the manifestation of a spontaneous symmetry breaking, which makes the system pass from a randomly distributed to a non-randomly distributed fibre mean angle.

A comparison between the theory proposed in this work with that of “standard” remodelling is reported in Figs. 5, 6, and 7, in which we highlighted the influence of \hat{W}_{rem} on the evolution in space and time of the mean angle and of the stress distribution within the considered sample of tissue.

Finally, we studied the influence of the parameter a , which features in the definition of $\hat{\alpha}_W$ (see (46)), on the spatiotemporal evolution of Q . We remark that, for $a = 0$, the free energy density \hat{W}_{AC} becomes a function of Q only, i.e., $\hat{W}_{\text{AC}}(Q) = \mathcal{A}_0/(\pi/4)^4 Q^2(Q - \pi/2)^2$, and is thus invariant under the discrete symmetry transformation $Q \mapsto \pi/2 - Q$. Such symmetry manifests itself through the shape of the curves in Fig. 8a. On the contrary, for $a \neq 0$, \hat{W}_{AC} loses this discrete symmetry because of the coupling with the deformation (see (28)). We conclude that our theory of remodelling is capable of describing the histological profile of the mean angle as the result of a spontaneous symmetry breaking, which occurs in the tissue independently on deformation (perhaps, when the tissue is generated) and proposes to interpret the coupling between the evolution of Q and the deformation as a further symmetry breaking (this time, however, a non-spontaneous one).

A last remark should be made in regards of the time scales involved in the considered remodelling process. Such time scales, indeed, are dictated in this work by the loading history imposed from the outside and, for this reason, they may appear unnatural. In fact, they represent a situation that is different from the more natural one in which the characteristic time scale of remodelling is the result of the coupling of this phenomenon with other processes, like e.g. growth, and with the deformations and stresses induced by those. Introducing growth in the description of remodelling presented in this work, and therefore determining the natural time scales of these phenomena, is one of the objectives of our studies.

Our long term goal is to employ the approach proposed in our work for characterising the structural evolution of fibrous tissues also in pathological situations. For example, collagen orientation in articular cartilage varies due to several reasons: It has been observed that, in a damaged or aged tissue [65, 66], the fibre orientation is quite far from that in the healthy tissue. In Fig. 9, the numerical results obtained in an unconfined compression test have been qualitatively compared with the experimental outcomes shown in [65]. The horizontal lines in the experimental figures mark each of the three zones of articular cartilage (deep, middle, superficial). We see that, in a stressed and damaged tissue, these three zones sensibly change, and in particular the deep zone becomes more extended along the depth of the tissue, while the middle zone shifts towards the top. A similar axial distribution of the remodelling variable can be obtained, by means of the remodelling law (62) presented in this work, at the end of a loading ramp in an unconfined compression. Naturally, this result should be enriched by accounting, for example, for the concurrent mass changes of both the collagen and the matrix, and for the reorganisation of the cells surrounding the fibres during realistic (either physiological or pathological) loading conditions borne by the tissue. Also this topic is subject of our current investigations.

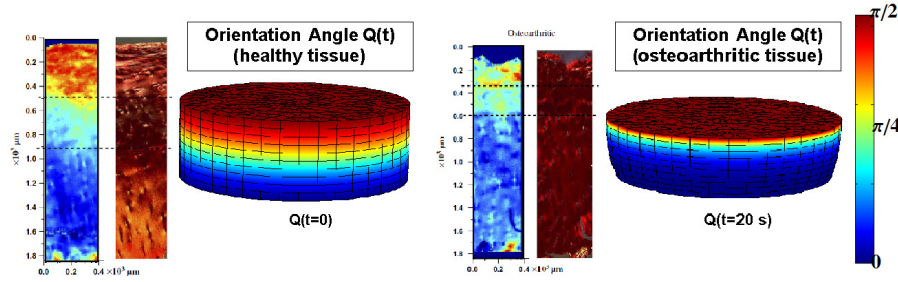


Fig. 9 Numerical simulations of an unconfined compression, in the unloaded initial configuration (left) and in the loaded condition at $t = T_{\text{ramp}}$ (deformed cylindrical shape on the right), have been qualitatively compared with the experimental results shown in [65]. The experimental observations (reported in the four columns featuring in the figure) correspond to a FT-IRIS image and a polarised light microscopy image (from left to right) directly taken from [65] (open access article). The four columns in the figure are reprinted from [65], Copyright (2005), with permission from Elsevier

Appendix A

To recall the relation between the operators in the physical space and those in the reference configuration of a body, we select an open subset $\mathcal{C} \subset \mathcal{B}$ of the reference configuration and we consider the map $\chi_t: \mathcal{C} \rightarrow \chi_t(\mathcal{C})$ that, at each time t , embeds \mathcal{C} into the open subset $\chi_t(\mathcal{C}) \subset \mathcal{S}$ of the physical space \mathcal{S} . Clearly, it applies that $\chi_t(X) = \chi(X, t)$ for all $X \in \mathcal{C}$ and for all t (cf.

Equation (1)). Then, let ${}^s f: \chi_t(\mathcal{C}) \rightarrow \mathbb{R}$ and ${}^s \mathbf{u}: \chi_t(\mathcal{C}) \rightarrow T\mathcal{S}$ be a scalar and a vector field, respectively, and let $f = {}^s f \circ \chi_t: \mathcal{C} \rightarrow \mathbb{R}$ and $\mathbf{u} = {}^s \mathbf{u} \circ \chi_t: \mathcal{C} \rightarrow T\mathcal{S}$ denote the counterparts of ${}^s f$ and ${}^s \mathbf{u}$ defined over \mathcal{C} . Thus, the identities $f(X) = {}^s f(\chi_t(X)) = {}^s f(x)$ and $\mathbf{u}(X) = {}^s \mathbf{u}(\chi_t(X)) = {}^s \mathbf{u}(x)$ hold true, with $x = \chi_t(X) \in \chi_t(\mathcal{C})$ and $X \in \mathcal{C}$. Hence, if all the partial derivatives of f and ${}^s f$ exist in \mathcal{C} and $\chi_t(\mathcal{C})$, respectively, enforcing the chain rule yields

$$\text{Grad } f = [\mathbf{F}^T \text{grad } {}^s f] \circ \chi_t \quad \Rightarrow \quad \text{grad } {}^s f = [\mathbf{F}^{-T} \text{Grad } f] \circ \chi_t^{-1}, \quad (72a)$$

$$\text{Grad } \mathbf{u} = [(\text{grad } {}^s \mathbf{u}) \circ \chi_t] \mathbf{F} \quad \Rightarrow \quad (\text{grad } {}^s \mathbf{u}) \circ \chi_t = (\text{Grad } \mathbf{u})(\mathbf{F}^{-1} \circ \chi_t). \quad (72b)$$

The divergence of ${}^s \mathbf{u}$ is given by

$$\begin{aligned} (\text{div } {}^s \mathbf{u}) \circ \chi_t &= \text{tr}[(\text{grad } {}^s \mathbf{u}) \circ \chi_t] \\ &= \text{tr}[(\text{Grad } \mathbf{u})(\mathbf{F}^{-1} \circ \chi_t)] = (\text{Grad } \mathbf{u}) : \mathbf{F}^{-T}. \end{aligned} \quad (73)$$

Note that in (72a), (72b), and (73) the explicit dependence of \mathbf{F} on time is omitted but understood, and that, in the definitions of f and \mathbf{u} , time t plays the role of a parameter.

Given a differentiable material vector field $\mathbf{U}: \mathcal{C} \rightarrow T\mathcal{B}$, the divergence of \mathbf{U} in \mathcal{C} reads

$$\text{Div } \mathbf{U} = \text{tr}[\text{Grad } \mathbf{U}]. \quad (74)$$

If ${}^s \mathbf{u}$ is the flux vector associated with some scalar physical quantity, then the material counterpart of ${}^s \mathbf{u}$ is defined through the Piola transformation $\mathbf{U} = J(\mathbf{F}^{-1} \circ \chi_t) \mathbf{u}$, with $\mathbf{u} = {}^s \mathbf{u} \circ \chi_t$, and the divergences $\text{div } {}^s \mathbf{u}$ and $\text{Div } \mathbf{U}$ are related through [41]

$$J(\text{div } {}^s \mathbf{u}) \circ \chi_t = \text{Div } \mathbf{U}. \quad (75)$$

In the sequel, the compositions with χ_t and χ_t^{-1} will be omitted for the sake of a lighter notation.

The definitions reported above can be generalised to the computation of the gradient and divergence of tensor fields of any order (see e.g. [41] for details). If, for example, ${}^s \mathbf{t}$ is a second-order tensor field defined over $\chi_t(\mathcal{C}) \subset \mathcal{S}$ and characterised by contravariant components, its gradient, $\text{grad } {}^s \mathbf{t}$, is a third-order tensor field with two contravariant indices (i.e., those corresponding to the first pair of indices) and one covariant index (i.e., that individuated by the direction along which the covariant differentiation is performed), while its divergence, $\text{div } {}^s \mathbf{t}$, is the unique vector field satisfying $\text{div}({}^s \mathbf{t}^T \cdot \mathbf{h}) = (\text{div } {}^s \mathbf{t}) \cdot \mathbf{h}$, for all constant spatial vectors \mathbf{h} . In components, $\text{div } {}^s \mathbf{t}$ reads $(\text{div } {}^s \mathbf{t})^a = ({}^s \mathbf{t})^{ab}_{;b}$, where the semicolon “;” stands for partial covariant differentiation.

Often, the notation $\text{grad } {}^s f$ and $\text{div } {}^s \mathbf{u}$ is replaced by $\text{grad } {}^s f \equiv \nabla {}^s f$ and $\text{div } {}^s \mathbf{u} \equiv \nabla \cdot {}^s \mathbf{u}$ (accordingly, for the material description, one writes $\text{Grad } f \equiv \nabla_R f$ and $\text{Div } \mathbf{U} \equiv \nabla_R \cdot \mathbf{U}$, the subscript “_R” meaning that the differentiation is done in the reference configuration). In this paper, however, for the sake of consistency with the notation adopted in previous works, we prefer to use the

symbols “grad” and “div” for the operators in the physical space and “Grad” and “Div” for the operators in the reference configuration. Moreover, in the differential geometric approach that we follow, the symbol nabla, ∇ , is usually reserved to a *connection*, i.e., a *covariant derivative*. While ∇ and grad could be used interchangeably, the use of “ $\nabla \cdot$ ” for div becomes cumbersome as it relies on the traditional abuse of notation according to which ∇ is a “vector”, which does *not* fit with covariant differentiation.

Appendix B

Within a purely mechanical framework (i.e., in the absence of thermal effects), and under the hypothesis that the mass densities of the solid and the fluid phase are constant, the dissipation inequality, written per unit volume of the tissue’s reference configuration, can be cast in the form

$$\begin{aligned} \mathfrak{D}_0 = & -\dot{W} + \mathbf{P}_s : \mathbf{g}\dot{\mathbf{F}} + \mathbf{P}_f : \mathbf{g} \text{Grad} \mathbf{v}_f - J\boldsymbol{\pi}_f \cdot \mathbf{w} \\ & + \mathcal{R}_{\text{int}}\dot{Q} + \text{Div}(-T\bar{\boldsymbol{\Sigma}}^\eta) \geq 0. \end{aligned} \quad (76)$$

Equation (76) is obtained by specialising the theoretical framework developed, for example, by Hassanizadeh [67], Bennethum et al. [68], and Grillo et al. [22] to the setting presented in our work. In the definition of \mathfrak{D}_0 , W is the overall energy density of the solid phase, expressed per unit volume of the reference configuration and defined in (31a), $\mathbf{P}_s : \mathbf{g}\dot{\mathbf{F}}$ and $\mathbf{P}_f : \mathbf{g} \text{Grad} \mathbf{v}_f$ are the internal mechanical power densities produced by the agency of the first Piola-Kirchhoff stress tensors \mathbf{P}_s and \mathbf{P}_f on $\dot{\mathbf{F}}$ and $\text{Grad} \mathbf{v}_f$, respectively, $J\boldsymbol{\pi}_f \cdot \mathbf{w}$ is the power density related to the interaction force between the fluid and the solid phase, i.e., $\boldsymbol{\pi}_f$, which is conjugate to the relative velocity $\mathbf{w} = \mathbf{v}_f - \mathbf{v}_s$, $\mathcal{R}_{\text{int}}\dot{Q}$ is the internal power density associated with remodelling, T is absolute temperature, and $\bar{\boldsymbol{\Sigma}}^\eta$ is the entropy flux vector. We remark that, since thermal effects are excluded from the present context, T is here understood as a constant reference temperature, which provides $T\bar{\boldsymbol{\Sigma}}^\eta$ with the physical units of energy flux vector.

We notice that, in the Classical Thermodynamics of Irreversible Processes, the entropy flux vector is usually defined by dividing the heat flux vector by the absolute temperature [69]. Therefore, if this hypothesis is accepted, there can be no entropy flux vector in a theory in which thermal effects—and, consequently, the heat flux vector—are disregarded from the outset. However, within a more general setting, the entropy flux vector of a thermodynamic theory need not be related *a priori* to the heat flux vector [55]. In fact, this is the case studied in our work, which is non-classical in the sense that the free energy density of the solid phase depends on the gradient of the fibre mean angle, Q , as well as on Q itself. Hence, if the approach outlined by Jamet [55] is adopted, one might introduce the entropy flux vector $\bar{\boldsymbol{\Sigma}}^\eta$ even in a purely mechanical framework, in which, thus, the heat flux vector is absent, and determine a constitutive representation for it. This is, in fact, the path followed in our work.

To show the calculations leading to the definitions of the terms reported in (30a)–(30d), i.e., \mathfrak{D}_I , \mathfrak{D}_{II} , \mathfrak{D}_{III} , and \mathfrak{D}_{IV} , we modify (76) as

$$\begin{aligned} \mathfrak{D} = \mathfrak{D}_0 + p \left[\Phi_s \mathbf{F}^{-T} : \dot{\mathbf{F}} + (J - \Phi_s) \mathbf{F}^{-T} : \text{Grad} \mathbf{v}_f \right. \\ \left. + (J \mathbf{g}^{-1} \text{grad} \phi_f) \cdot \mathbf{w} \right] \geq 0, \end{aligned} \quad (77)$$

where p is pressure, and the sum of the terms in brackets expresses the mass balance law for the system as a whole, i.e.,

$$\Phi_s \mathbf{F}^{-T} : \dot{\mathbf{F}} + (J - \Phi_s) \mathbf{F}^{-T} : \text{Grad} \mathbf{v}_f + (J \mathbf{g}^{-1} \text{grad} \phi_f) \cdot \mathbf{w} = 0. \quad (78)$$

We recall that (78) is obtained by adding together the mass balance laws for the solid and the fluid phase, which, in the case of constant mass densities, can be written as

$$D_s \phi_s + \phi_s \text{div} \mathbf{v}_s = 0, \quad (79a)$$

$$D_s \phi_f + (\text{grad} \phi_f) \cdot \mathbf{w} + \phi_f \text{div} \mathbf{v}_f = 0, \quad (79b)$$

and computing the backward Piola transform of the result.

In writing (77), the mass balance law of the mixture as a whole is treated as a constraint of the theory, and the pressure p is thus the Lagrange multiplier associated with it. Moreover, since the terms between brackets in (77) add up to zero, \mathfrak{D} and \mathfrak{D}_0 are numerically equal to each other, although they acquire a rather different meaning. For a discussion on the subject, the Reader is referred to [68].

By substituting the expression of \mathfrak{D}_0 in (77), the dissipation inequality becomes

$$\begin{aligned} \mathfrak{D} = -\dot{W} + \left[\mathbf{P}_s + \Phi_s p \mathbf{g}^{-1} \mathbf{F}^{-T} \right] : \mathbf{g} \dot{\mathbf{F}} \\ + \left[\mathbf{P}_f + (J - \Phi_s) p \mathbf{g}^{-1} \mathbf{F}^{-T} \right] : \mathbf{g} \text{Grad} \mathbf{v}_f \\ - J [\boldsymbol{\pi}_f - p \mathbf{g}^{-1} \text{grad} \phi_f] \cdot \mathbf{w} \\ + \mathcal{R}_{\text{int}} \dot{Q} + \text{Div}(-T \bar{\boldsymbol{\Omega}}^\eta) \geq 0. \end{aligned} \quad (80)$$

Then, we expand the time derivative of W , thereby obtaining

$$\begin{aligned} \dot{W} &= \frac{\partial \hat{W}}{\partial \mathbf{C}} : \dot{\mathbf{C}} + \frac{\partial \hat{W}}{\partial Q} \dot{Q} + \frac{\partial \hat{W}}{\partial \text{Grad} Q} \overline{\text{Grad} \dot{Q}} \\ &= \frac{\partial \hat{W}}{\partial \mathbf{C}} : \dot{\mathbf{C}} + \frac{\partial \hat{W}}{\partial Q} \dot{Q} + \frac{\partial \hat{W}}{\partial \text{Grad} Q} \text{Grad} \dot{Q} \\ &= \mathbf{F} \left(2 \frac{\partial \hat{W}}{\partial \mathbf{C}} \right) : \mathbf{g} \dot{\mathbf{F}} + \text{Div} \left[\frac{\partial \hat{W}}{\partial \text{Grad} Q} \dot{Q} \right] \\ &\quad + \left[\frac{\partial \hat{W}}{\partial Q} - \text{Div} \left(\frac{\partial \hat{W}}{\partial \text{Grad} Q} \right) \right] \dot{Q}. \end{aligned} \quad (81)$$

Finally, by replacing the right-hand-side of (81) into (80), and grouping together all the terms that multiply the same generalised velocity, we find

$$\begin{aligned}
\mathfrak{D} = & \left\{ -\mathbf{F} \left(2 \frac{\partial \hat{W}}{\partial \mathbf{C}} \right) + \mathbf{P}_s + \Phi_s p \mathbf{g}^{-1} \mathbf{F}^{-\text{T}} \right\} : \mathbf{g} \dot{\mathbf{F}} \\
& + \left\{ \mathbf{P}_f + (J - \Phi_s) p \mathbf{g}^{-1} \mathbf{F}^{-\text{T}} \right\} : \mathbf{g} \text{Grad} \mathbf{v}_f \\
& - J [\boldsymbol{\pi}_f - p \mathbf{g}^{-1} \text{grad} \phi_f] \cdot \mathbf{w} \\
& + \left\{ \mathcal{R}_{\text{int}} - \left[\frac{\partial \hat{W}}{\partial Q} - \text{Div} \left(\frac{\partial \hat{W}}{\partial \text{Grad} Q} \right) \right] \right\} \dot{Q} \\
& + \text{Div} \left[- \frac{\partial \hat{W}}{\partial \text{Grad} Q} \dot{Q} - T \bar{\boldsymbol{\Sigma}}^\eta \right] \geq 0.
\end{aligned} \tag{82}$$

Thus, the terms \mathfrak{D}_I , \mathfrak{D}_{II} , \mathfrak{D}_{III} , and \mathfrak{D}_{IV} can be identified by comparing (82) with (30a)–(30d). In principle, \mathfrak{D}_I accounts for the dissipative stresses associated with the solid and the fluid phase, respectively. However, since in our work the solid phase is assumed to be hyperelastic, and the fluid is assumed to be macroscopically inviscid, neither the solid nor the fluid phase feature a dissipative stress. Hence, \mathfrak{D}_I must vanish identically. The term \mathfrak{D}_{II} is the dissipation due to the solid-fluid interactions. In fact, the brackets multiplying \mathbf{w} define the dissipative part of the interaction force density $\boldsymbol{\pi}_f$, which leads to Darcy’s law. Analogously, \mathfrak{D}_{III} consists of the dissipation related to the process of remodelling, and the coefficient of \dot{Q} determines the dissipative part of the internal remodelling generalised force \mathcal{R}_{int} . Finally, \mathfrak{D}_{IV} is assumed to vanish in the present context, thereby defining the entropy flux vector $\bar{\boldsymbol{\Sigma}}^\eta$.

We emphasise that the framework within which the dissipation inequality is studied in our work is based on the hypothesis of validity of Darcy’s law for the description of the fluid filtration velocity. Moreover, neither the dissipative effects related to the mixture viscosity [70] nor those connected with the microstructure viscosity of the considered medium [70] are taken into account. These, however, can be relevant in the poroelastic approach to bone structure developed in [70]. In addition, for increasing magnitude of the tissue’s permeability, also a possible deviation from the flow regime predicted by Darcy’s law can be appreciable. Indeed, when this is the case, the Brinkman correction should be included into the model [70].

Acknowledgements We would like to thank Dr. Lorenzo Tentarelli for useful discussions.

In Memoriam

In memory of our master, Prof. Gaetano Giaquinta (1945–2016), who inspired this work back in 2004, by suggesting the use of the Ginzburg-Landau energy.

Compliance with Ethical Standards

The authors declare that they have no conflict of interest.

References

1. Cowin SC (2000) How is a tissue built? *J Biomech Engng* 122:553–569.
2. Holzapfel GA, Gasser TC, Ogden RW (2000) A new constitutive framework for arterial wall mechanics and a comparative study of material models. *J Elast* 61:1–48
3. Holzapfel GA, Gasser TC (2001) A viscoelastic model for fiber-reinforced composites at finite strains: continuum basis, computational aspects and applications. *Comput Methods Appl Mech Eng* 190:4379–4403
4. Merodio J, Ogden RW (2005) Mechanical response of fiber-reinforced incompressible non-linearly elastic solids. *Int J Non-Linear Mech*,40:213–227
5. Merodio J (2006) On constitutive equations for fiber-reinforced nonlinearly viscoelastic solids. *Mech Res Commun* 33:764–770
6. deBotton G, Schmucl G (2009) Mechanics of composites with two families of finitely extensible fibers undergoing large deformations. *J Mech Phys Solids* 57:1165–1181
7. Lanir Y (1983) Constitutive equations for fibrous connective tissues. *J Biomech* 16:1–12
8. Gasser TC, Ogden RW, Holzapfel GA (2006) Hyperelastic modelling of arterial layers with distributed collagen fibre orientations. *J R Soc Interface* 3:15–35
9. Federico S, Herzog W (2008) On the anisotropy and inhomogeneity of permeability in articular cartilage. *Biomech Model Mechanobiol* 7:367–378
10. Federico S, Gasser TC (2010) Non-linear elasticity of biological tissues with statistical fibre orientation. *J R Soc Interface*, 7:955–966
11. Menzel A (2005) Modelling of anisotropic growth in biological tissues. *Biomech Model Mechanobiol* 3:147–171
12. Menzel A (2007) A fibre reorientation model for orthotropic multiplicative growth. Configurational driving stresses, kinematics-based reorientation and algorithmic aspects. *Biomech Model Mechanobiol* 6(5):303–320
13. Maroudas A, Bullough P (1968) Permeability of articular cartilage. *Nature* 219:1260–1261
14. Federico S, Herzog W (2008) Towards an analytical model of soft tissues. *J Biomech* 41:3309–3313
15. Federico S, Herzog W (2008) On the permeability of fibre-reinforced porous materials. *Int J Solids Struct* 45:2160–2172
16. Federico S, Grillo A (2012) Elasticity and permeability of porous fibre-reinforced materials under large deformations. *Mech Mater* 44:58–71
17. Aspden RM, Hukins DWL (1981) Collagen organization in articular cartilage, determined by X-ray diffraction, and its relationship to tissue function. *Proc R Soc Lond B Biol Sci* 212:299–304
18. Mollenhauer J, Aurich M, Muehleman C, Khelashvili G, Irving TC (2003) X-ray diffraction of the molecular substructure of human articular cartilage. *Connect Tissue Res* 44:201–207
19. Di Carlo A and Quiligotti S (2002) Growth and balance. *Mech Res Commun* 29:449–456
20. Fung YC (1990) *Biomechanics. Motion, Flow, Stress, and Growth*. Springer-Verlag, New York, USA
21. Taber LA (1995) *Biomechanics of growth, remodeling and morphogenesis*. ASME Appl Mech Rev 48:487–545
22. Grillo A, Federico S, Wittum G (2012) Growth, mass transfer, and remodeling in fiber-reinforced, multi-constituent materials. *Int J Nonlinear Mech* 47:388–401
23. Grillo A, Wittum G, Tomic A, Federico S (2015) Remodelling in statistically oriented fibre-reinforced materials and biological tissues. *Math Mech Solids* 20(9):1107–1129
24. Ginzburg VL, Landau LD (1950) On the theory of superconductivity. *Zh. Eksp. Teor. Fiz.* 20:1064–1082 [published in English in: Landau LD Collected papers, Pergamon Press, Oxford, UK (1965) p. 546]
25. Ginzburg VL (2003) On superconductivity and superfluidity. Nobel Lecture 96–127
26. Allen SM, Cahn JW (1979) A macroscopic theory for antiphase boundary motion and its application to antiphase domain coarsening. *Acta Metall* 27:1085–1095
27. Olsson T, Klarbring A (2008) Residual stresses in soft tissue as a consequence of growth and remodeling: application to an arterial geometry. *Eur J Mech A-Solid* 27:959–974

28. Cermelli P, Fried E, Sellers S (2001) Configurational stress, yield and flow in rate-independent plasticity. *Proc R Soc Lond A* 457:1447–1467
29. Barocas VH, Tranquillo RT (1997) An anisotropic biphasic theory of tissue-equivalent mechanics: The interplay among cell traction, fibrillar network deformation, fibril alignment, and cell contact guidance. *J Biomech Eng* 119:137–145
30. Kroon M (2010) A continuum mechanics framework and a constitutive model for remodelling of collagen gels and collagenous tissues. *J Mech Phys Solids* 58:918–933
31. Imatani S, Maugin GA (2002) A constitutive model for material growth and its application to three-dimensional finite element analysis. *Mech Res Comm* 29:477–483
32. Driessen NJB, Peters GWM, Huyghe JM, Bouten CVC, Baaijens FPT (2003) Remodelling of continuously distributed collagen fibres in soft connective tissues. *J Biomech* 36(8):1151–1158
33. Ohsumi TK, Flaherty JE, Evans MC, Barocas VH (2008) Three-dimensional simulation of anisotropic cell-driven collagen gel compaction. *Biomechan Model Mechanobiol* 7:53–62
34. Schrieff AJ, Zeindlinger G, Pierce DM, Regitnig P, Holzapfel GA (2012) Determination of the layer-specific distributed collagen fibre orientations in human thoracic and abdominal aortas and common iliac arteries. *J R Soc Interface* 9:1275–1286
35. Gasser TC, Gallinetti S, Xing X, Forsell C, Swedenborg J, Roy J (2012) Spatial orientation of collagen fibers in the abdominal aortic aneurysm's wall and its relation to wall mechanics. *Acta Biomater* 8:3091–3103
36. Tsamis A, Krawiec JT, Vorp DA (2013) Elastic and collagen fibre microstructure of the human aorta in ageing and disease: A review. *J R Soc Interface* 10(83):1–22
37. Quiligotti S, Maugin GA, dell'Isola F (2003) An eshelbian approach to the nonlinear mechanics of constrained solid-fluid mixtures. *Acta Mech* 160:45–60
38. Tomic A, Grillo A, Federico S (2014) Poroelastic materials reinforced by statistically oriented fibres - numerical implementation and application to articular cartilage. *IMA J Appl Math* 79:1027–1059
39. Grillo A, Guaily A, Giverso C, Federico S (2015) Non-linear model for compression tests on articular cartilage. *J Biomech Eng* 137:071004–1–071004–8
40. Carfagna M, Grillo A (2017) The spherical design algorithm in the numerical simulation of biological tissues with statistical fibre-reinforcement. *Comput Visual Sci* <https://doi.org/10.1007/s00791-017-0278-6>
41. Marsden JE, Hughes TJR (1983) *Mathematical Foundations of Elasticity*. Dover Publications, Inc., New York
42. Baaijens F, Bouthen C, Driessen N (2010) Modeling collagen remodeling. *J Biomech* 43:166–175
43. Ateshian GA, Weiss JA Anisotropic hydraulic permeability under finite deformation. *J Biomech Eng* 132:111004–1–111004–7
44. Rivlin RS, Ericksen JL (1955) Stress-deformation relations for isotropic materials. *J Rational Mech Anal* 4:323–425
45. Liu I-S (1982) On representations of anisotropic invariants. *Int J Eng Sci* 20(10):1099–1109
46. Holmes MH, Mow VC (1990) The nonlinear characteristics of soft gels and hydrated connective tissues in ultrafiltration. *J Biomech* 23:1145–1156
47. Hill R (1963) Elastic properties of reinforced solids: some theoretical principles. *J Mech Phys Solids* 11:357–372
48. Walpole LJ (1969) On the overall elastic moduli of composite materials. *J Mech Phys Solids* 17:235–251
49. Weng GJ (1990) The theoretical connection between Mori-Tanaka's theory and the Hashin-Shtrikman-Walpole bounds. *Int J Eng Science* 28:1111–1120
50. Alhasadi MF, Federico S (2017) Relation between Eshelby stress and Eshelby fourth-order tensor within an ellipsoidal inclusion. *Acta Mech* 228:1045–1069
51. Eshelby JD (1957) The determination of the elastic field of an ellipsoidal inclusion, and related problems. *Proc R Soc Lond A* 241:376–396
52. Almeida ES, Spilker RL (1998) Finite element formulations for hyperelastic transversely isotropic biphasic soft tissues. *Comput Methods Appl Mech Eng* 151:513–538
53. Felsager B (1998) *Geometry, Particles, and Fields*. Springer, Heidelberg, Germany

54. Federico S, Grillo A, La Rosa G, Giaquinta G, Herzog W (2005) A transversely isotropic, transversely homogeneous microstructural-statistical model of articular cartilage. *J Biomech* 38:2008–2018
55. Jamet D (2001) Diffuse interface models in fluid mechanics. *Adv Water Resour* 25(3):335–348
56. Macklin P, Lowengrub J (2007) Nonlinear simulation of the effect of microenvironment on tumor growth. *J Theor Biol* 245:677–704
57. Wise SM, Lowengrub JS, Frieboes HB, Cristini V (2008) Three-dimensional multispecies nonlinear tumor growth—I model and numerical method. *J Theor Biol* 253:524–543
58. Cristini V, Li X, Lowengrub JS, Wise SM (2009) Nonlinear simulations of solid tumor growth using a mixture model: invasion and branching. *J Math Biol* 58:723–763
59. Wu JZ, Herzog W (2000) Finite element simulation of location- and time-dependent mechanical behavior of chondrocytes in unconfined compression tests. *Ann Biomed Eng* 28:318–330
60. Mow VC, Holmes MH, Lai MW (1984) Fluid transport and mechanical properties of articular cartilage: a review. *J Biomech* 17:377–394
61. Pins GD, Huang EK, Christiansen DL, Silver FH (1997) Effects of static axial strain on the tensile properties and failure mechanisms of self-assembled collagen fibers. *J Appl Polym Sci* 63(11):1429–1440
62. Hariton I, deBotton G, Gasser TC, Holzapfel GA (2007) Stress-driven collagen fiber remodeling in arterial walls. *Biomech Model Mechanobiol* 6(3):163–175
63. Hardin RH, Sloane NJA (1996) McLaren’s improved snub cube and other new spherical designs in three dimensions. *Discrete Comput Geom* 15:429–441
64. Paetzold H, Goepfert C, Huber G, Hoenig E, Pörtner R, Schilling AF, Meenen NM, Morlock MM (2012) The development of the collagen fibre network in tissue-engineered cartilage constructs in vivo. engineered cartilage reorganises fibre network. *Eur Cell Mater* 23:209–221
65. Bi X, Li G, Doty SB, Camacho NP (2005) A novel method for determination of collagen orientation in cartilage by Fourier transform infrared imaging spectroscopy (ft-iris.) *Osteoarthr Cartilage* 13:1050–1058
66. Julkunen P, Harjula T, Iivarinen J, Marjanen J, Seppänen T, Närhi T, Arokoski J, Lammi MJ, Brama PA, Jurvelin JS, Helminen HJ (2009) Biomechanical, biochemical and structural correlations in immature and mature rabbit articular cartilage. *Osteoarthr Cartilage* 17(12):1628–1638
67. Hassanizadeh SM (1986) Derivation of basic equations of mass transport in porous media. Part 2. Generalized Darcy’s and Fick’s laws. *Adv Water Resour* 9:208–222
68. Bennethum LS, Murad MA, Cushman JH (2000) Macroscale thermodynamics and the chemical potential for swelling porous media. *Transport Porous Med* 39:187–225
69. Mićunović MV (2009) Thermomechanics of Viscoplasticity — Fundamentals and Applications. Springer, Heidelberg, Germany
70. Giorgio I, Andreus U, Scerrato D, dell’Isola F (2016) A visco-poroelastic model of functional adaptation in bones reconstructed with bio-resorbable materials. *Biomech Model Mechanobiol* 15(5):1325–1343